

Observational signatures of neutron stars in low-mass X-ray binaries climbing a stability peak

E. M. Kantor¹ \star , M. E. Gusakov^{1,2}, A. I. Chugunov¹

¹*Ioffe Physical-Technical Institute of the Russian Academy of Sciences, Polytekhnicheskaya 26, 194021 St.-Petersburg, Russia*

²*Peter the Great St.Petersburg Polytechnic University, Polytekhnicheskaya 29, 195251 St.-Petersburg, Russia*

Accepted 2015 xxxx. Received 2015 xxxx; in original form 2015 xxxx

ABSTRACT

In the recent papers by Gusakov et al. (2014b,a) a new scenario describing evolution of rapidly rotating neutron stars in low-mass X-ray binaries was proposed. The scenario accounts for a resonant interaction of normal r modes with superfluid inertial modes at some specific internal stellar temperatures (“resonance temperatures”). This interaction results in an enhanced damping of r mode and appearance of the “stability peaks” in the temperature – spin frequency plane, which split the r-mode instability window in the vicinity of the resonance temperatures. The scenario suggests that the hot and rapidly rotating NSs spend most of their life climbing up these peaks and, in particular, are observed there at the moment. We analyze in detail possible observational signatures of this suggestion. In particular, we show that these objects may exhibit ‘anti-glitches’ – sudden frequency jumps on a time scale of hours-months.

Key words: stars: neutron – stars: interiors – pulsars

1 INTRODUCTION

Neutron stars (NSs) are compact rotating relativistic objects. Rotation allows NSs to harbor inertial oscillation modes, the most interesting representatives of which are r modes. As it was shown by Andersson (1998) and Friedman & Morsink (1998), in the absence of dissipation r modes are subject to a gravitational driven instability (the CFS instability) at *any* NS spin frequency ν . An account for dissipative processes stabilizes NSs to some extent, resulting in the appearance of the so called “instability window” in the $T^\infty - \nu$ plane, where T^∞ is the redshifted internal stellar temperature. A typical instability window is shown in panel (a) of Fig. 1. In the region filled with gray NSs are stable (we call it “stability region”), in the white region they are unstable (it is “instability window”).

Observations of NSs in low mass X-ray binaries (LMXBs) revealed that many NSs fall well outside the stability region (see circles with error bars in panel (a) of Fig. 1 and Ho, Andersson, & Haskell 2011; Haskell, Degenaar, & Ho 2012; Gusakov, Chugunov, & Kantor 2014a,b). At the same time, NS evolution models predict that a probability to find an NS in the instability window is negligibly small (Levin 1999; Heyl 2002). This apparent contradiction was addressed in a number of papers (e.g., Andersson & Kokkotas 2001; Haskell, Degenaar, & Ho 2012; Ho, Andersson, & Haskell 2011; Mahmoodifar & Strohmayer 2013; Haskell, Glampedakis, & Andersson 2014; Alford, Han, & Schwenzer 2015) which attempted to reconcile theory with observations (see Ho et al. 2011; Haskell et al. 2012; Gusakov et al. 2014a; Haskell 2015 for a short review of the existing ideas). In this paper we explore observational consequences of one such idea (Gusakov et al. 2014b,a) which, as we believe, allows one to explain the existing observations rather naturally.

Gusakov et al. (2014b,a) argued that a simultaneous account for superfluidity of nucleons in the cores of NSs and finite-temperature effects substantially modifies the NS oscillation spectra and leads to a resonance interaction of r mode with superfluid inertial modes at some certain NS temperatures T_{res}^∞ (called “resonance temperatures” in what follows). This resonance interaction stabilizes r modes in the vicinity of T_{res}^∞ . As a result, stability peaks appear in the $T^\infty - \nu$ plane. A typical instability window constructed allowing for the resonance interaction of the modes is demonstrated in panel (b) of Fig. 1 (the figure is taken from Gusakov et al. 2014a where it is discussed in detail). The evolution track of an NS in such instability

\star kantor@mail.ioffe.ru

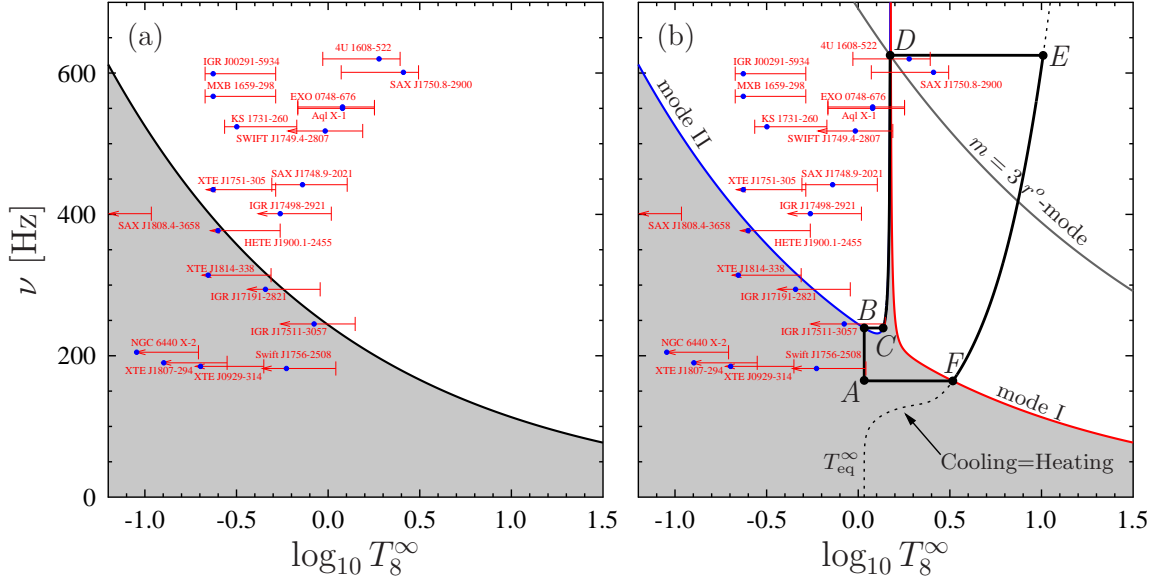


Figure 1. Panel (a) shows ‘standard’ NS instability window (white region) in the $T^\infty - \nu$ plane, where $T_8^\infty \equiv T^\infty/(10^8 \text{ K})$. A region where NSs are stable (i.e. r-modes are not excited) is filled with grey. Circles with error bars show observational data for NSs in LMXBs with measured ν and estimated T^∞ . Panel (b) presents an example of the instability window (figure 5 of Gusakov et al. 2014a) plotted allowing for the resonance interaction of r mode with superfluid inertial modes. The stability peak CD appears because of this interaction. Evolution of the spin frequency ν and internal redshifted temperature T^∞ is shown by thick solid line (the track $A-B-C-D-E-F-A$). See Gusakov et al. 2014a for more details.

window was studied by Gusakov et al. (2014b,a) and is shown here by the solid thick line. It was found by Gusakov et al. (2014b,a) that an NS spends substantial amount of time climbing up the left edge of the stability peak so that the probability to find it there is high. This presents a natural explanation for the existence of numerous NSs in the region that was thought to be unstable with respect to r-mode excitation — they climb up the stability peak.

Detailed analyzes of the evolution track revealed (Gusakov et al. 2014a) that it undergoes small oscillations (in what follows we will call them α -oscillations) near the edge of the peak (unresolved on the scale of Fig. 1)¹. These oscillations can, in principle, be detected and this paper discusses their possible observational manifestations.

The paper is organized as follows. In Section 2 we present basic equations governing evolution of NSs in LMXBs, then in Section 3 we analyze α -oscillation properties of a star climbing up/down the stability peak. In Section 4 we estimate different parameters of α -oscillations (e.g., oscillation period). Section 5.1 analyzes peculiar timing behavior of an NS attached to the stability peak. In Section 5.2 we discuss whether gravitational radiation from such stars can be detected. Section 6 inspects existing observations. We conclude in Section 7.

2 GENERAL EQUATIONS

The equations describing evolution of NSs in LMXBs consist of (for more details see, e.g., Owen et al. 1998; Ho & Lai 2000; Gusakov et al. 2014a):

(i) Thermal balance equation

$$C_{\text{tot}} \frac{dT^\infty}{dt} = W_{\text{Diss}} - L_{\text{cool}} + K_n \dot{M} c^2, \quad (1)$$

which describes evolution of internal redshifted temperature T^∞ of the star (we assume it is uniform throughout the core). In equation (1) C_{tot} is the total heat capacity of an NS; L_{cool} is the thermal luminosity of the star due to neutrino emission from the interior and photon emission from its surface. The term $K_n \dot{M} c^2$ describes deep crustal heating due to nuclear transformations of accreted matter (see Brown, Bildsten, & Rutledge 1998); K_n characterizes the efficiency of this heating (following Brown 2000 and Bondarescu et al. 2007 we adopt here $K_n = 10^{-3}$); \dot{M} is the accretion rate from the low-mass companion, in what follows we will assume that it is constant and equals to the accretion rate averaged over quiescent and

¹ Similar oscillations (in different context) were discussed by Levin (1999) and Wagoner, Hennawi, & Liu (2001).

active phases, $\langle \dot{M} \rangle$; c is the speed of light. Finally, W_{Diss} in equation (1) is the rate of the energy release in the course of dissipative damping of the excited r mode; it is given by

$$W_{\text{Diss}} = \frac{\tilde{J}MR^2\Omega^2\alpha^2}{\tau_{\text{Diss}}}, \quad (2)$$

where M and R are the NS mass and radius, respectively. In all numerical calculations we adopt $M = 1.4M_{\odot}$ and $R = 10$ km. $\Omega = 2\pi\nu$ is the NS spin frequency (measured in s^{-1}); α is the dimensionless amplitude of the r mode (for definition of α see, e.g., formula 1 of Gusakov et al. 2014a); τ_{Diss} is the r -mode damping timescale due to various dissipative processes (shear and bulk viscosities, Ekman layer dissipation, mutual friction etc., see Andersson & Kokkotas 2001). In the range of temperatures relevant to LMXB systems the most powerful mechanisms of r -mode dissipation not too close to the stability peak are the shear viscosity and dissipation in the Ekman layer.² Due to large uncertainties inherent to Ekman-layer calculations (see, e.g., Levin & Ushomirsky 2001; Yoshida & Lee 2001; Andersson & Kokkotas 2001; Rieutord 2001a,b; Mendell 2001; Kinney & Mendell 2003; Glampedakis & Andersson 2006) we, for definiteness, consider shear viscosity (to be more precise, electron shear viscosity) as the only dissipation mechanism for r -modes far from the resonances with superfluid inertial modes (see Gusakov et al. 2014a for an expanded discussion and justification of our choice). Note that near the resonances (on the slopes of the stability peaks) superfluid inertial modes admix to the r -mode solution (r -mode transforms into a superfluid inertial mode and vice versa) so that dissipation there is mainly determined by the mutual friction mechanism, which is extremely efficient for superfluid modes (Lindblom & Mendell 2000). Finally, \tilde{J} in equation (2) is a numerical coefficient, which equals $\tilde{J} \approx 1.6353 \times 10^{-2}$ for an r mode with multipolarity $l = m = 2$ and the polytropic equation of state (EOS) with polytropic index $n = 1$ ($P \propto \rho^{1+1/n}$, where P and ρ are, respectively, the pressure and density of matter).

(ii) Evolution of stellar spin frequency Ω ,

$$\frac{d\Omega}{dt} = -\frac{2Q\alpha^2\Omega}{\tau_{\text{Diss}}} + \dot{\Omega}_{\text{ext}}, \quad (3)$$

where the first term in the right-hand side represents NS spin down due to r -mode dissipation; $Q = l(l+1)\tilde{J}/(4\tilde{I})$; \tilde{I} is defined as $I = \tilde{I}MR^2$ (I is stellar moment of inertia). For polytropic EOS with $n = 1$ one has $\tilde{I} \approx 0.261$; $\dot{\Omega}_{\text{ext}}$ in equation (3) is the rate of change of the NS spin frequency due to other spin down mechanisms, such as accretion torque, magneto-dipole radiation, gravitational wave emission by possible mountains on an NS etc.

(iii) Evolution of r -mode amplitude α

$$\frac{d\alpha}{dt} = -\alpha \left(\frac{1}{\tau_{\text{GR}}} + \frac{1}{\tau_{\text{Diss}}} \right), \quad (4)$$

where τ_{GR} is the gravitational radiation timescale, which is negative, because emission of gravitational waves excites r mode. For polytropic EOS with $n = 1$ it can be calculated as (see Andersson & Kokkotas 2001)

$$\tau_{\text{GR}} = -\tau_{\text{GR}0} \left(\frac{M}{1.4M_{\odot}} \right)^{-1} \left(\frac{R}{10 \text{ km}} \right)^{-2l} \left(\frac{\nu}{1 \text{ kHz}} \right)^{-2l-2}, \quad (5)$$

where $\tau_{\text{GR}0} \approx 46.4$ s for $l = m = 2$ r mode. Instability window is given by the condition $|\tau_{\text{GR}}| < \tau_{\text{Diss}}$, which means that excitation of r modes occurs faster than their damping. The boundary of the instability window defines the instability curve at which $|\tau_{\text{GR}}| = \tau_{\text{Diss}}$. Note, that we kept only the leading order terms in α in Equations (2)–(4), assuming that $\alpha \ll 1$; we also neglected the term $\propto \dot{\Omega}_{\text{ext}}/\Omega$ in Equation (4), because $\dot{\Omega}_{\text{ext}}/\Omega \ll |1/\tau_{\text{GR}}|$. Moreover, Equations (1)–(4) are only valid as soon as oscillations are linear, that is they are far from the saturation defined either by non-linear coupling to other oscillation modes (see, e.g., Bondarescu, Teukolsky, & Wasserman 2007) or by some other non-linear processes such as those discussed by Haskell, Glampedakis, & Andersson (2014) and Alford, Han, & Schwenzer (2015).

These equations can be rewritten in a more compact form as

$$\frac{dT^{\infty}}{dt} = F_1(T^{\infty}, \Omega)\Omega^2 A - F_2(T^{\infty}), \quad (6)$$

$$\frac{d\Omega}{dt} = -G(T^{\infty}, \Omega)A\Omega + \dot{\Omega}_{\text{ext}}, \quad (7)$$

$$\frac{dA}{dt} = -AH(T^{\infty}, \Omega), \quad (8)$$

where $A \equiv \alpha^2$,

$$F_1(T^{\infty}, \Omega) \equiv \frac{\tilde{J}MR^2}{C_{\text{tot}}\tau_{\text{Diss}}}, \quad (9)$$

$$F_2(T^{\infty}) \equiv \frac{L_{\text{cool}} - K_n \dot{M}c^2}{C_{\text{tot}}}, \quad (10)$$

² Here we do not discuss any ‘exotic’ dissipation processes such as bulk viscosity due to hyperons or quarks.

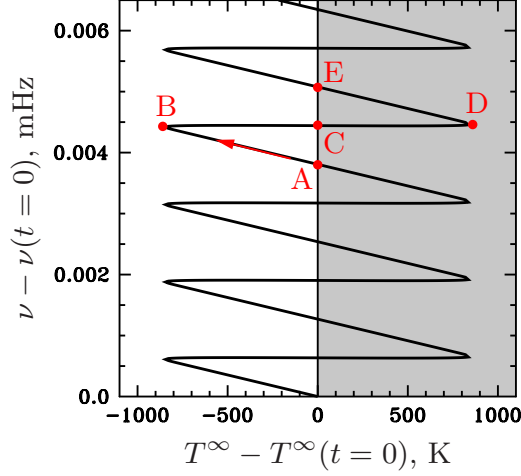


Figure 2. Oscillations of the evolutionary track near the instability curve. Shown are variations of the rotation frequency (in millihertz) and internal temperature (in Kelvins) starting from some initial moment of time $t = 0$ for the source 4U 1608-522. The time interval is ~ 3 years, direct Urca processes are forbidden, see Section 5 for details.

$$G(T^\infty, \Omega) \equiv \frac{2Q}{\tau_{\text{Diss}}}, \quad (11)$$

$$H(T^\infty, \Omega) \equiv 2 \left(\frac{1}{\tau_{\text{GR}}} + \frac{1}{\tau_{\text{Diss}}} \right). \quad (12)$$

Equations (6)–(8) fully describe evolution of NSs in LMXBs. In what follows we will use them for the analysis of oscillations of NS evolution tracks near the left edge of the stability peak, mentioned in Section 1. An example of such oscillations is presented in Fig. 2, which is a zoomed in fragment of the track in the vicinity of the stability peak, analogous to that shown in panel (b) of Fig. 1. The region filled with grey is the stability region inside the peak, almost vertical straight line is the instability curve (the left edge of the peak). Zigzag is the evolutionary track. At point A of the cycle the r mode amplitude has the lowest value which is not sufficient to keep a star at the given temperature. Thus the NS cools down, crosses the instability curve and enters the instability region where r mode starts to grow. As the r mode amplitude increases, the heating by the dissipation of the excited r mode becomes more and more efficient and slows down the NS cooling rate. At some moment the NS reaches “thermal balance” point (point B in Fig. 2), where heating by the accretion and r-mode dissipation exactly compensates NS cooling. Further increase of the r-mode amplitude leads to a temperature growth, that brings the star to the instability curve. After NS crosses the instability curve (point C), the r-mode rise replaces with the r-mode decay, and NS heating reduces. When a thermal balance point is reached again (now it is point D), further decreasing of r-mode amplitude results in a net NS cooling. As the NS cools down to the instability curve (point E), the cycle repeats. In what follows, to avoid confusion with the r-mode oscillations, we will call these oscillations α -oscillations (emphasizing that it is the oscillations of the r-mode amplitude α). In the next section α -oscillations are described analytically.

3 α -OSCILLATIONS NEAR THE EDGE OF THE STABILITY PEAK

In what follows, to simplify notations the redshifted internal stellar temperature T^∞ will be denoted by T . Unlike the oscillation amplitude squared, A , which varies significantly in the course of α -oscillations, the variations of T and Ω (or ν) are small. Thus, for the analysis of α -oscillations we will present T and Ω as a sum of the equilibrium solution (see below) which we will denote by the subscript 0, and a small perturbation near this solution,

$$T = T_0 + \delta T, \quad (13)$$

$$\Omega = \Omega_0 + \delta \Omega. \quad (14)$$

The equilibrium solution assumes that $\Omega = \Omega_0$, $T = T_0$, and $A = A_0$ do not oscillate and the star track follows the left edge of the stability peak, which is defined by the condition

$$H(T_0, \Omega_0) = 0. \quad (15)$$

It gives us the dependence $\Omega_0(T_0)$. The time dependence of these quantities is driven by the following equations (cf. equations 6 and 7)

$$\frac{dT_0}{dt} = F_1(T_0, \Omega_0)\Omega_0^2 A_0 - F_2(T_0), \quad (16)$$

$$\frac{d\Omega_0}{dt} = -G(T_0, \Omega_0)A_0\Omega_0 + \dot{\Omega}_{\text{ext}}, \quad (17)$$

hence

$$\frac{\Omega_0}{T_0} \frac{dT_0}{d\Omega_0} = -\frac{F_1(T_0, \Omega_0)\Omega_0^3 A_0 - F_2(T_0)\Omega_0}{G(T_0, \Omega_0)A_0\Omega_0 T_0 - \dot{\Omega}_{\text{ext}} T_0}. \quad (18)$$

This equation should be understood as an equation for A_0 , because $dT_0/d\Omega_0$ is known from Equation (15). Generally $(\Omega_0/T_0)dT_0/d\Omega_0 \lesssim 1$, while the ratio of the terms $F_1(T_0, \Omega_0)\Omega_0^3 A_0$ and $G(T_0, \Omega_0)A_0\Omega_0 T_0$, entering the right-hand-side of Equation (18), can be estimated as

$$\frac{F_1(T_0, \Omega_0)\Omega_0^2}{G(T_0, \Omega_0)T_0} = \frac{2I\Omega_0^2}{l(l+1)C_{\text{tot}}T_0}, \quad (19)$$

that is it is of the order of the ratio of rotational energy to the thermal energy. In the range of Ω_0 and T_0 relevant to LMXBs, this ratio is $\sim 10^5 \gg 1$. At the same time, the external torque $\dot{\Omega}_{\text{ext}}$ in Equation (18) is generally (at not too small A_0) comparable to the torque due to r modes, $G(T_0, \Omega_0)A_0\Omega_0$. This means that to satisfy Equation (18) A_0 , to a very good approximation, should be given by the thermal equilibrium condition,

$$F_1(T_0, \Omega_0)\Omega_0^2 A_0 \approx F_2(T_0). \quad (20)$$

Substituting now Equations (13) and (14) into (6)–(8) one obtains the following system of equations for r-mode oscillation amplitude squared, A , and perturbations δT and $\delta\Omega$ (note that the quantity A strongly deviates from its equilibrium value A_0 , while perturbations δT and $\delta\Omega$ are small so that only first-order terms $\propto \delta T$ and $\delta\Omega$ are retained in these equations)

$$\begin{aligned} \frac{d\delta T}{dt} = & F_1(T_0, \Omega_0)\Omega_0^2(A - A_0) + \left(\frac{\partial F_1(T, \Omega)}{\partial T} \Big|_{T_0, \Omega_0} \Omega_0^2 A - \frac{\partial F_2(T)}{\partial T} \Big|_{T_0} \right) \delta T \\ & + \left(2F_1(T_0, \Omega_0)\Omega_0 A + \frac{\partial F_1(T, \Omega)}{\partial \Omega} \Big|_{T_0, \Omega_0} \Omega_0^2 A \right) \delta\Omega, \end{aligned} \quad (21)$$

$$\begin{aligned} \frac{d\delta\Omega}{dt} = & -G(T_0, \Omega_0)\Omega_0(A - A_0) - \frac{\partial G(T, \Omega)}{\partial T} \Big|_{T_0, \Omega_0} \Omega_0 A \delta T \\ & - \left(\frac{\partial G(T, \Omega)}{\partial \Omega} \Big|_{T_0, \Omega_0} \Omega_0 A + G(T_0, \Omega_0)A \right) \delta\Omega, \end{aligned} \quad (22)$$

$$\frac{dA}{dt} = -A \left(\frac{\partial H(T, \Omega)}{\partial T} \Big|_{T_0, \Omega_0} \delta T + \frac{\partial H(T, \Omega)}{\partial \Omega} \Big|_{T_0, \Omega_0} \delta\Omega \right). \quad (23)$$

This system does not depend on the external torque $\dot{\Omega}_{\text{ext}}$ explicitly (only by means of A_0 , which is a function of $\dot{\Omega}_{\text{ext}}$), thus it is valid for both ascending-the-peak and descending-the-peak NSs, and is even valid in the absence of accretion (that is, for millisecond pulsars, if they are attached to a peak or for hot widows/HOFNARs, see Chugunov, Gusakov, & Kantor 2014). Generally, the underlined terms are small, because T and Ω only slightly deviate from their equilibrium values, while, as we already mentioned above, the deviation of r-mode amplitude squared, A , is not small. Thus the leading terms in Equations (21) and (22) are those proportional to $A - A_0$. Dividing now Equation (21) by Equation (22) and keeping the leading terms only, one can estimate [(cf. Equation (19))]

$$\frac{\Omega_0}{T_0} \frac{\delta T}{\delta\Omega} \sim \frac{F_1(T_0, \Omega_0)\Omega_0^2}{G(T_0, \Omega_0)T_0} \sim 10^5 \gg 1. \quad (24)$$

Thus it is easy to verify that the terms in the system of Equations (21)–(23) $\propto \delta\Omega$ are small and can be skipped (then the equation for $\delta\Omega$ decouples and can be disregarded in what follows). We are left then with

$$\frac{d\delta T}{dt} = F_1(T_0, \Omega_0)\Omega_0^2(A - A_0) + \left(\frac{\partial F_1(T, \Omega)}{\partial T} \Big|_{T_0, \Omega_0} \Omega_0^2 A - \frac{\partial F_2(T)}{\partial T} \Big|_{T_0} \right) \delta T, \quad (25)$$

$$\frac{dA}{dt} = -A \frac{\partial H(T, \Omega)}{\partial T} \Big|_{T_0, \Omega_0} \delta T. \quad (26)$$

The time derivative of the Equation (26) is:

$$\frac{d}{dt} \frac{d \log A}{dt} = -\frac{\partial H(T, \Omega)}{\partial T} \Big|_{T_0, \Omega_0} \frac{d\delta T}{dt} - \frac{d}{dt} \frac{\partial H(T, \Omega)}{\partial T} \Big|_{T_0, \Omega_0} \delta T. \quad (27)$$

Substituting now $d\delta T/dt$ from Equation (25) into (27), we obtain

$$\frac{d^2 y}{dt^2} = -\beta(A - A_0) - \frac{\partial H(T, \Omega)}{\partial T}|_{T_0, \Omega_0} \gamma(A) \delta T - \frac{d}{dt} \frac{\partial H(T, \Omega)}{\partial T}|_{T_0, \Omega_0} \delta T, \quad (28)$$

where we introduced a new variable $y = \log A$ and defined

$$\beta \equiv \frac{\partial H(T, \Omega)}{\partial T}|_{T_0, \Omega_0} F_1(T_0, \Omega_0) \Omega_0^2, \quad (29)$$

$$\gamma(A) \equiv \frac{\partial F_1(T, \Omega)}{\partial T}|_{T_0, \Omega_0} \Omega_0^2 A - \frac{\partial F_2(T)}{\partial T}|_{T_0}. \quad (30)$$

The third term in the right-hand-side of equation (28) is much smaller than the second one, because $\partial H(T, \Omega)/\partial T|_{T_0, \Omega_0}$ evolves on a timescale of peak climbing (spin-up timescale), $\gtrsim 10^8$ yr, which is much longer than $\gamma^{-1} \sim t_{\text{cool}}$, where t_{cool} is the cooling timescale, $t_{\text{cool}} \approx T_0/F_2(T_0) \lesssim 10^6$ yr. Thus, we will omit the third term in what follows,

$$\frac{d^2 y}{dt^2} = -\beta(A - A_0) - \frac{\partial H(T, \Omega)}{\partial T}|_{T_0, \Omega_0} \gamma(A) \delta T. \quad (31)$$

Substituting now δT from equation (26) into (31), we arrive at

$$\frac{d^2 y}{dt^2} = -\beta(e^y - e^{y_0}) + \gamma(A) \frac{dy}{dt}, \quad (32)$$

where $y_0 \equiv \log A_0$. Equation (32) describes *nonlinear* oscillations of the squared amplitude A near the equilibrium point $A = A_0$ with dissipation/excitation described by the last term, which is typically small.

Note that the quantity A , averaged over the period \hat{P} of α -oscillations, equals $\langle A \rangle = A_0$, i.e., the equilibrium r-mode amplitude $\alpha_0 \equiv \sqrt{A_0}$ is, at the same time, the root mean square of α . Indeed, the integral of the function δT over \hat{P} should vanish (we ignore a negligible change of the equilibrium temperature T_0 on a timescale of \hat{P}),

$$\int^{\hat{P}} d(\delta T) = 0. \quad (33)$$

On the other hand

$$\int^{\hat{P}} d(\delta T) = \int^{\hat{P}} \frac{d(\delta T)}{dt} dt = \int^{\hat{P}} F_1(T_0, \Omega_0) \Omega_0^2 (A - A_0) dt, \quad (34)$$

where use has been made of (25) with the last small term $\propto \delta T$ omitted. Thus, because T_0 and Ω_0 are almost constants on a timescale of α -oscillation period,

$$\int^{\hat{P}} A dt = A_0 \hat{P} \quad (35)$$

or $\langle A \rangle = A_0$.

To study α -oscillations driven by equation (32), it is convenient to introduce a notion of the “energy” \hat{E} for this equation [this function is conserved, $\dot{\hat{E}} = 0$, when $\gamma = 0$; then it is just the first integral of Equation (32)],

$$\hat{E} \equiv \frac{1}{2} \dot{y}^2 + \beta(e^y - y e^{y_0}). \quad (36)$$

Equation (32) is equivalent to the following formula,

$$\dot{\hat{E}} = \gamma(A) \dot{y}^2, \quad (37)$$

so that the energy variation averaged over the α -oscillation period, \hat{P} , is

$$\langle \dot{\hat{E}} \rangle = \langle \gamma(A) \dot{y}^2 \rangle = \frac{1}{\hat{P}} \int^{\hat{P}} \gamma(A) \dot{y}^2 dt, \quad (38)$$

If $\langle \dot{\hat{E}} \rangle$ is negative α -oscillations are damped, otherwise they are excited. As long as dissipation/excitation is weak, y in this integral can be calculated from Equation (32) with $\gamma(A) = 0$. Equivalently, y can be found from Equations (25) and (26) with the last term [= $\gamma(A)\delta T$] in equation (25) omitted. To analyze integral in Equation (38) let us notice that [see also (34)]

$$\begin{aligned} 0 &= \int^{\hat{P}} d(\delta T^3) = \int^{\hat{P}} \frac{d(\delta T^3)}{dt} dt = 3 \int^{\hat{P}} \delta T^2 \frac{d(\delta T)}{dt} dt \\ &= 3 \int^{\hat{P}} \left(\frac{\dot{y}}{\frac{\partial H(T, \Omega)}{\partial T}|_{T_0, \Omega_0}} \right)^2 F_1(T_0, \Omega_0) \Omega_0^2 (A - A_0) dt, \end{aligned} \quad (39)$$

where use has been made of Equations (25) (with the last term neglected) and (26). Since T_0 and Ω_0 are almost constants on

a timescale of α -oscillation period, corresponding quantities can be factored out of the integral, yielding

$$\int^{\hat{P}} A \dot{y}^2 dt = A_0 \int^{\hat{P}} \dot{y}^2 dt. \quad (40)$$

Hence,

$$\begin{aligned} \langle \dot{\hat{E}} \rangle &= \frac{1}{\hat{P}} \int^{\hat{P}} \gamma(A) \dot{y}^2 dt = \frac{1}{\hat{P}} \int^{\hat{P}} \left(\frac{\partial F_1}{\partial T} |_{T_0, \Omega_0} \Omega_0^2 A - \frac{\partial F_2}{\partial T} |_{T_0} \right) \dot{y}^2 dt \\ &= \frac{1}{\hat{P}} \left(\frac{\partial F_1}{\partial T} |_{T_0, \Omega_0} \Omega_0^2 A_0 - \frac{\partial F_2}{\partial T} |_{T_0} \right) \int^{\hat{P}} \dot{y}^2 dt = \frac{1}{\hat{P}} \gamma(A_0) \int^{\hat{P}} \dot{y}^2 dt, \end{aligned} \quad (41)$$

which means that when $\gamma(A_0)$ is negative we have dissipation of α -oscillations; in the opposite case α -oscillations excite.

Notice, that the value of $\gamma(A_0)$ depends on the geometry of the stability peak — for wider peaks the derivative $-\partial\tau_{\text{diss}}/\partial T|_{T_0, \Omega_0}$, and hence $\partial F_1(T, \Omega)/\partial T|_{T_0, \Omega_0}$ [see Equation (9)], is smaller. It results in decrease of $\gamma(A_0)$ with increasing peak width; for sufficiently wide peaks $\gamma(A_0)$ is negative and α -oscillations are damped.

The same criterion follows from the analysis of the linear oscillations (when $A - A_0 \ll A_0$). The stability of the solution to the system of linear equations

$$\frac{d\delta T}{dt} = F_1(T_0, \Omega_0) \Omega_0^2 \delta A + \gamma(A_0) \delta T, \quad (42)$$

$$\frac{d\delta A}{dt} = -A_0 \frac{\partial H(T, \Omega)}{\partial T} |_{T_0, \Omega_0} \delta T \quad (43)$$

requires $\gamma(A_0) < 0$ and $F_1(T_0, \Omega_0) \Omega_0^2 A_0 \frac{\partial H(T, \Omega)}{\partial T} |_{T_0, \Omega_0} > 0$. The last condition is satisfied automatically at the left edge of the peak, while the first one coincides with the stability condition in the non-linear case. This coincidence was not necessary: A system, unstable in the linear approximation, can, in principle, have stable non-linear solutions (and vice versa). We can conclude that in the case when

$$\gamma(A_0) > 0 \quad (44)$$

a star cannot move along the peak without α -oscillations. In all numerical examples considered below this inequality is satisfied. We note that a similar criterion was obtained, in the linear approximation, by Wagoner et al. (2001). This reference analyzed stability of an NS track in the vicinity of the instability curve (positive, negative and horizontal slopes of the instability curve were discussed).

The above consideration allowed α to vary without limits. However, the r-mode oscillation amplitude cannot *increase* infinitely. It is limited by the saturation amplitude α_{sat} , which is determined by a non-linear interaction of r mode with other oscillation modes, or some other nonlinear processes such as those discussed by Haskell et al. (2014) and Alford et al. (2015)³. The value of α_{sat} is rather uncertain, but in what follows we will assume, in accordance with Bondarescu et al. (2007), that it is of the order of 10^{-4} , i.e., we take $\alpha_{\text{sat}} = 10^{-4}$ ($y_{\text{sat}} = -18.4$). Similarly, the oscillation amplitude α cannot *decrease* infinitely. The minimum value of α is defined by some spontaneous excitation mechanism, that can be either of thermal origin or induced, e.g., by accretion. For example, for internal temperature $T = 10^8$ K r-mode energy becomes comparable to $k_B T$ (k_B is the Boltzmann constant) at the threshold value $\alpha_{\text{th}} \sim 10^{-29}$. This value seems to be too small to be a real lower limit for α , thus, in what follows, we adopt $\alpha_{\text{th}} = \alpha_{\text{th}}^{\text{fid}} = 10^{-12}$ as a fiducial value for illustration of our results. Qualitatively, our main results are not sensitive to α_{th} [see a discussion after Eq. (47) and the footnote 4].

Strictly speaking, the derivation of the criterion (44) is valid only while $\alpha_{\text{th}} < \alpha < \alpha_{\text{sat}}$ during the whole oscillation period. When α in the course of oscillations reaches the value of α_{th} or α_{sat} , the above derivation is not applicable. Then each α -oscillation cycle starts with the same initial condition at the left edge of the peak: It can be either $\alpha = \alpha_{\text{th}}$ (in this case the star enters the instability window after the cycle starts, see point *A* in Fig. 2) or $\alpha = \alpha_{\text{sat}}$ (in this case the star penetrates the stability region inside the peak after the cycle starts, see point *C* in Fig. 2); in both cases the cycle “does not remember” the prehistory (initial conditions are the same for any such cycle). For illustration, let us consider a cycle with the initial condition $\alpha = \alpha_{\text{th}}$. In the beginning of the cycle (point *A* in Fig. 2) the star is at the instability curve and $y = y_{\text{th}}$ [$y_{\text{th}} = \log(\alpha_{\text{th}}^2)$], $\hat{E} = \beta(e^{y_{\text{th}}} - y_{\text{th}} e^{y_0})$ ($\dot{y} = 0$ at the instability curve). If we forget for a moment about “non-conservation” of the energy \hat{E} during the cycle, then $\hat{E} = \text{const}$, and y can reach its initial value y_{th} only when \dot{y} will vanish again, that is at the instability curve (point *E* in Fig. 2). The result of the energy injection into α -oscillations will be that y will reach again the initial value y_{th} not exactly at the instability curve, as strict energy conservation would imply, but a little bit earlier

³ Note that the equation (32) is only valid if $\alpha < \alpha_{\text{sat}}$. For example, if the saturation is defined by the nonlinear mode coupling, this condition means that α should be lower than the parametric instability thresholds for all nonlinear mode couplings. For larger r-mode amplitudes the nonlinear mode coupling leads to excitation of daughter modes, and this excitation should be described properly (see, e.g., Brink et al. 2004; Bondarescu et al. 2007, 2009). For definiteness, we apply a simplified model, assuming that r mode saturation fixes amplitude α (and thus y) at a constant value $\alpha = \alpha_{\text{sat}}$ ($y = y_{\text{sat}}$) (see, e.g., Gusakov et al. 2014a for more details).

(the r-mode amplitude wants to decrease further, hence increasing the range of y variation, but y is limited by y_{th}). This is, however, not important for the next cycle, which again starts with $y = y_{\text{th}}$ and will be exactly the same as the previous one. A similar analysis can be carried out for the situation when y_{sat} limits the amplitude growth. Notice that, anyway, satisfaction of the condition (44) implies that α -oscillations are inevitable, and they will grow until they reach α_{th} or α_{sat} .

4 SOME OSCILLATION PARAMETERS

In the course of fully developed α -oscillations r mode amplitude α varies in some range $\alpha_{\text{min}} < \alpha < \alpha_{\text{max}}$, with either $\alpha_{\text{min}} = \alpha_{\text{th}}$ ($\alpha_{\text{max}} < \alpha_{\text{sat}}$) or $\alpha_{\text{max}} = \alpha_{\text{sat}}$ ($\alpha_{\text{min}} > \alpha_{\text{th}}$). Typically, if α_{sat} is not too low, the former scenario is realized. Let us estimate the value of α_{max} in this case. The ‘energy’ of oscillations (36) in the beginning of the cycle, when $y = y_{\text{th}}$ at the instability curve, equals (note that at that moment $\dot{y} = 0$)

$$\widehat{E} = \beta(e^{y_{\text{th}}} - y_{\text{th}}e^{y_0}). \quad (45)$$

Then NS penetrates the instability region where y increases, r mode heats the star and eventually NS reaches the instability curve with the maximum (over the period) value of y , given by $y = y_{\text{max}}$. Correspondingly, the energy can be written as (again, we have $\dot{y} = 0$ at the instability curve)

$$\widehat{E} = \beta(e^{y_{\text{max}}} - y_{\text{max}}e^{y_0}). \quad (46)$$

As have already been discussed above, the energy of oscillations is conserved approximately on a timescale of α -oscillation period (i.e. dissipation/excitation of oscillations is small). Hence one can equate Equations (45) and (46) and get, neglecting $e^{y_{\text{th}}}$ in comparison to other terms,

$$\alpha_{\text{max}} \approx \sqrt{y_{\text{max}} - y_{\text{th}}} \alpha_0 \equiv k \alpha_0. \quad (47)$$

(We recall that $y_{\text{max}} = \log \alpha_{\text{max}}^2$.) Since $|y_{\text{max}}| \ll |y_{\text{th}}|$ the coefficient $k = \sqrt{y_{\text{max}} - y_{\text{th}}}$ depends mostly on α_{th} and is not sensitive to, e.g., peak and/or stellar parameters. For the value $\alpha_{\text{th}} = 10^{-12}$, adopted in this paper, the coefficient k varies, depending on α_0 , in the range $k \approx (5 \div 6)$. Lower value of α_{th} would lead to a higher difference between α_{max} and α_0 ; for example, for $\alpha_{\text{th}} = 10^{-29}$ (unrealistically small value) k varies in the range $k \approx (10.3 \div 10.7)$. On the opposite, higher value of α_{th} would lead to a smaller difference between α_{max} and α_0 ; for example, $\alpha_{\text{th}} = 10^{-10}$ would give $k \approx (4 \div 5)$.

In the case when α_{sat} , rather than α_{th} , is reached in the course of α -oscillations [this situation takes place when α_{max} , given by Equation (47), is greater than α_{sat}], energy conservation equation,

$$e^{y_{\text{min}}} - y_{\text{min}}e^{y_0} = e^{y_{\text{sat}}} - y_{\text{sat}}e^{y_0}, \quad (48)$$

would provide us with the value of $\alpha_{\text{min}} > \alpha_{\text{th}}$. Neglecting the small term $e^{y_{\text{min}}}$ in (48), it gives

$$\alpha_{\text{min}} \approx \alpha_{\text{sat}} \exp\left(-\frac{\alpha_{\text{sat}}^2}{2\alpha_0^2}\right). \quad (49)$$

Here we will not discuss this situation in detail.

Let us now estimate the time, τ , that an NS spends near $\alpha_{\text{max}} < \alpha_{\text{sat}}$. For that we expand $y(t)$ in the vicinity of y_{max} (near the instability curve) in the Taylor series,

$$y \approx y_{\text{max}} + \frac{1}{2}\ddot{y}t^2 \quad (50)$$

(we remind that $\dot{y} = 0$ at the instability curve). From Equation (50) it follows that α will decrease by a factor of $e \approx 2.71$ in time τ given by

$$\tau \approx \sqrt{-\frac{4}{\ddot{y}}}. \quad (51)$$

Using Equation (32) one can express \ddot{y} as $\ddot{y} \approx -\beta e^{y_{\text{max}}}$ (we neglect e^{y_0} in comparison with $e^{y_{\text{max}}}$ and ignore a small dissipative term $\propto \gamma(A)$ in that equation). Employing then the condition of the approximate heat balance (20), we get

$$\tau \approx \frac{2}{\sqrt{\beta A_{\text{max}}}} \approx \frac{2}{k \sqrt{\frac{\partial H(T, \Omega)}{\partial T}|_{T_0, \Omega_0} F_2(T_0)}}. \quad (52)$$

Depending on the parameters, τ is, typically, of the order of hours-months (see Tables 2–4).

The period of α -oscillations, \widehat{P} , is typically much longer than τ . It is easy to see it from the following rough estimate of the root-mean-square value of α ,

$$\alpha_0^2 \sim \frac{\alpha_{\text{max}}^2 \tau}{\widehat{P}}, \quad (53)$$

where we assumed that $\alpha = \alpha_{\text{max}}$ during the time τ , and the rest of the period $\alpha = 0$. Equation (53) gives $\widehat{P} \sim k^2 \tau$ [we

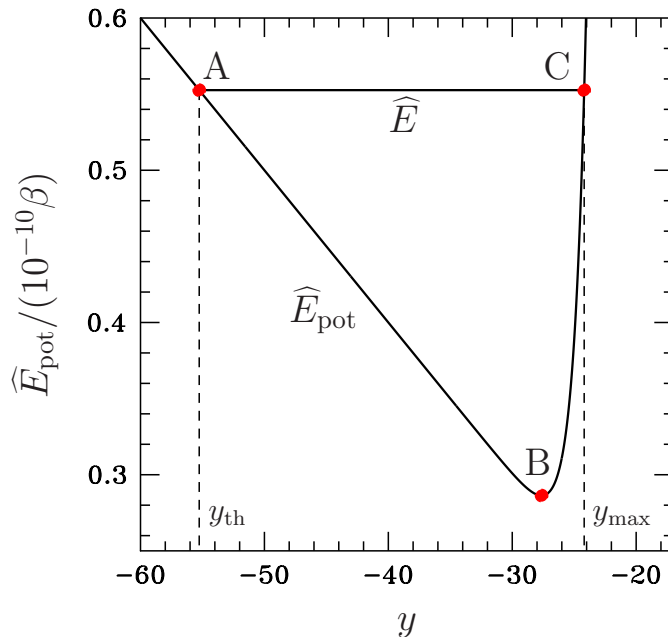


Figure 3. The “potential energy” $\widehat{E}_{\text{pot}}(y)$ normalized to $10^{-10}\beta$ as a function of y . The horizontal line shows the total energy $\widehat{E}/(10^{-10}\beta)$. The α -oscillations proceed between points A and C.

remind that $k \approx (5 \div 6)$ for $\alpha_{\text{th}} = 10^{-12}$]. Let us now estimate \widehat{P} more accurately. The energy (36) can be interpreted as a sum of “kinetic energy” $\dot{y}^2/2$ and “potential energy”,

$$\widehat{E}_{\text{pot}} = \beta(e^y - y e^{y_0}). \quad (54)$$

The dependence $\widehat{E}_{\text{pot}}(y)$ is shown in Fig. 3 (curve ABC). The straight horizontal line corresponds to the energy \widehat{E} normalized to $10^{-10}\beta$. For this plot we used $\alpha_0 = 10^{-6}$ and $\alpha_{\text{th}} = 10^{-12}$. The evolution of y and \dot{y} in this potential is as follows. At the time $t = 0$ one has $y = y_{\text{th}}$ and $\dot{y} = 0$ (point A in Fig. 2 and in Fig. 3). Then y increases, and $\dot{y} = 0$ increases as well. When y is sufficiently small the evolution proceeds in practically linear potential (stage A–B in Fig. 3) so that

$$\widehat{E}_{\text{pot}} \approx -\beta y e^{y_0}. \quad (55)$$

Then, eventually (around point B), r mode amplitude excites for a time period of the order of τ (which is short in comparison to \widehat{P}), and \widehat{E}_{pot} increases strongly, because the first term in (54) becomes important (stage B–C). Sharp rise of the potential energy (B–C stage) results in the “velocity” \dot{y} decrease down to zero in point C (corresponds to point C in Fig. 2). After that \dot{y} becomes negative, end evolution of y follows in the opposite direction (C–B–A stages in Fig. 3, which correspond to C–D–E stages in Fig. 2). The short stages B–C and C–B are analogous to the elastic bounce of a ball from the wall. Point B in Fig. 3 corresponds to the minimum of the expression (54) which is reached at $y = y_0$ (thus the point B of Fig. 3 coincides with the points B and D in Fig. 2). The potential energy drop at the stage A–B can be estimated with the formula (55) as

$$\Delta \widehat{E}_{\text{pot}} \approx -\beta e^{y_0} (y_0 - y_{\text{th}}). \quad (56)$$

Correspondingly, the velocity at point B equals

$$\dot{y}_B = \sqrt{2\beta e^{y_0} (y_0 - y_{\text{th}})}, \quad (57)$$

where we made use of the energy conservation. The evolution of y at the stage A – B is driven by the approximate equation [we neglect the first term in Equation (54) at this stage],

$$\frac{d^2 y}{dt^2} = \beta e^{y_0}. \quad (58)$$

Integrating this equation, one gets

$$\frac{dy}{dt} \approx \beta e^{y_0} t + C \quad (59)$$

with $C = 0$ due to the initial condition $\dot{y} = 0$. Using Equations (57) and (59), one can calculate the duration of the A–B stage,

$$t_{\text{AB}} \approx \frac{\dot{y}_{\text{B}}}{\beta e^{y_0}} \approx \sqrt{2(y_0 - y_{\text{th}})} \frac{\alpha_{\text{max}}}{\alpha_0} \frac{\tau}{2} = \sqrt{2(k^2 - \log k^2)} k \frac{\tau}{2}, \quad (60)$$

where the equality (52) has been used. Then the period of α -oscillations can be calculated as

$$\hat{P} \approx 2t_{\text{AB}} \approx \sqrt{2(k^2 - \log k^2)} k \tau. \quad (61)$$

It is the sum of durations of A–B and B–A (after reflection in point C) stages. The B–C and C–B stages proceed much faster (the typical duration of these stages $\sim \tau \ll \hat{P}$) and the corresponding contributions to \hat{P} can be neglected. Notice, that the ratio \hat{P}/τ depends on k only, which is in turn mainly determined by y_{th} , and is not sensitive to the stellar and peak parameters. The period \hat{P} varies in the range $\hat{P} \approx (33 \div 48)\tau$ for $k = 5 \div 6$ (typical values for $\alpha_{\text{th}} = 10^{-12}$). Thus, most of the time r mode is practically not excited and increases up to α_{max} for a short time interval of the order of τ ($\sim 1/40$ of the oscillation period).

5 OBSERVATIONAL CONSEQUENCES

In the course of α -oscillations (when moving along the stability peak) the temperature and spin frequency variations are very small, however, two quantities vary significantly. These are the r-mode amplitude, α , and spin frequency derivative, $\dot{\nu}$. Variation of α results in modulation of gravitational radiation while variation of $\dot{\nu}$ results in specific timing peculiarities of the signal from the star. In this section we analyze possible observational signatures of such variations.

In Tables 2–4 we introduce some parameters of α -oscillations for a number of NSs in LMXBs, which climb a peak within the scenario of Gusakov et al. (2014b,a). Unfortunately, up to now there are no calculations of temperature-dependent spectra of rotating superfluid NSs, so currently we do not know the exact resonance temperatures T_{res} and the widths of the stability peaks, characterized by the coupling parameter s (this parameter describes coupling of r modes with the superfluid inertial modes), see Gusakov et al. (2014a) for more details. Hence we will treat them as free parameters. We have some idea about the possible typical values of T_{res} and s from the calculations of temperature-dependent oscillation spectra of non-rotating NSs (Chugunov & Gusakov 2011; Kantor & Gusakov 2011; Gusakov et al. 2013; Gualtieri et al. 2014). Thus, in what follows we will choose them in the reasonable range indicated by these works. For illustration, we assume that each of the considered sources is attached to one of the four peaks, which are characterized by T_{res} and s . Two of these peaks are those described by Gusakov et al. (2014a), see figure 6 of that reference (one is centered at $T_{\text{res}} = 4.5 \times 10^7$ K and is plotted for the coupling parameter $s = 0.01$, another is centered at $T_{\text{res}} = 1.5 \times 10^8$ K and has $s = 0.001$), the other two are centered at $T_{\text{res}} = 7 \times 10^7$ K and $T_{\text{res}} = 10^8$ K with the coupling parameters $s = 0.01$ and $s = 0.001$, respectively. Notice that the lower temperature peaks have higher s , in agreement with the results of Gusakov et al. (2013) and Gualtieri et al. (2014). In our calculations the spin frequencies and surface effective temperatures for the observed sources were taken from the table I of Gusakov et al. (2014a) (if only an upper limit for the effective temperature is known, we take the latter to be equal to this upper limit).

α -oscillations depend on the NS cooling rate, which is rather uncertain, and can be enhanced strongly by the direct Urca (Durca) processes (see, e.g., Yakovlev et al. 2001). The most powerful of them is the neutron decay into proton and lepton (electron or muon) with the emission of anti-neutrino, $n \rightarrow p + l + \bar{\nu}_l$ (l stands for a lepton), and the corresponding inverse process, $p + l \rightarrow n + \nu_l$. However, these are the threshold processes which are forbidden at densities lower than some threshold densities. These thresholds are very sensitive to the EOS, and can be rather high. For some EOSs these processes are always forbidden, even for the most massive NS configurations (see, e.g., a recent model BSk19 by Potekhin et al. 2013). On the other hand, a majority of microscopic models predict that at a density $\rho \sim (2 - 3)\rho_0$ (ρ_0 is the nuclear density) hyperons should appear (see, e.g., Weissenborn et al. 2012; Bednarek et al. 2012; Gusakov et al. 2014c and references therein). In many of these models the first hyperon species to appear with growing density is Λ hyperons (see, e.g., Weissenborn et al. 2012; Bednarek et al. 2012; Gusakov et al. 2014c). Once Λ hyperons appear the Durca processes $\Lambda \rightarrow p + l + \bar{\nu}_l$ and $p + l \rightarrow \Lambda + \nu_l$ become possible. Although NS cooling due to these processes is slightly less efficient (Prakash et al. 1992; Yakovlev et al. 2001) than in the case of nucleonic (npl) Durca, these are *not* the threshold processes, and it is quite possible that they operate in NSs with lower masses than npl Durca processes (but the NS mass should be sufficiently high to host Λ hyperons in their cores). Both nucleonic and Λ hyperonic Durcas can be suppressed by baryon (i.e., proton, Λ hyperon, or neutron) superfluidity whose properties are very uncertain. However, it is very probable that protons are non-superfluid at high densities (see, e.g., Page et al. 2009), while critical temperatures of Λ hyperons are likely to be very low (Tanigawa et al. 2003; Takatsuka et al. 2006; Wang & Shen 2010), so that Λ -hyperonic Durca process is only weakly suppressed (or completely unsuppressed). On the other hand, the neutron superfluidity still can affect npl Durca. Neglecting possible suppression by superfluidity, the temperature dependence of the emission rate for both nucleonic and Λ hyperonic Durcas is the same, so that the emissivity due to Λ hyperonic Durca is equivalent to the emissivity due to npl Durca from the smaller stellar volume (namely, the radius of the central region of an NS, where Durca processes operate, R_{D} , should be smaller for npl Durca by approximately a factor

Table 1. NS parameters.

Source	ν , Hz	\dot{M}_{-10}		d , kpc		$T_{\text{S res}}$	s
4U 1608-522	620	3.6	Heinke et al. (2007)	4.1	Watts et al. (2008)	1.5	0.001
SAX J1750.8-2900	601	2.0	Lowell et al. (2012)	6.79	Watts et al. (2008)	1.5	0.001
EXO 0748-676	552	2.0	^a	7.4	Watts et al. (2008)	1.5	0.001
Aql X-1	550	4.0	Heinke et al. (2007)	4.55	Watts et al. (2008)	1.5	0.001
SWIFT J1749.4-2807	518	2.0	^b	6.7	Wijnands et al. (2009)	1.5	0.001
SAX J1748.9-2021	442	1.8	Heinke et al. (2007)	8.1	Watts et al. (2008)	1.0	0.001
IGR J17498-2921	401	2.0	^b	7.6	Linares et al. (2011)	1.0	0.001
KS 1731-260	524	1.5	^c	7.2	Watts et al. (2008)	0.7	0.01
IGR J00291-5934	599	0.05	^d	5	Watts et al. (2008)	0.45	0.01
MXB 1659-298	567	1.7	Heinke et al. (2007)	12	Watts et al. (2008)	0.45	0.01
XTE J1751-305	435	0.06	Heinke et al. (2009)	9	Watts et al. (2008)	0.45	0.01

^a Accretion rate is unknown (see, however, Degenaar et al. 2014). We adopt here the value $2.0 \times 10^{-10} \text{ M}_{\odot}/\text{yr}$.

^b Accretion rate is unknown. We adopt here the value $2.0 \times 10^{-10} \text{ M}_{\odot}/\text{yr}$.

^c Only an upper limit, $1.5 \times 10^{-9} \text{ M}_{\odot}/\text{yr}$ (accretion rate in active state), is known (Heinke et al. 2007). We adopt here the value $1.5 \times 10^{-10} \text{ M}_{\odot}/\text{yr}$.

^d We adopt here the value $5 \times 10^{-12} \text{ M}_{\odot}/\text{yr}$, somewhat in between the accretion rate from the paper by Heinke et al. (2009) ($2.5 \times 10^{-12} \text{ M}_{\odot}/\text{yr}$, which is too low to balance even the photon cooling from the NS surface) and the accretion rate from the paper by Patruno (2010), $(7-8) \times 10^{-12} \text{ M}_{\odot}/\text{yr}$.

of $(m_{\Lambda}^* r_{\Lambda\text{p}}/m_n^*)^{1/3} \approx 0.36$, see Appendix A). Thus, just to illustrate the effect of an enhanced NS cooling on the oscillations, we considered three cases: (i) all Durca processes are forbidden (Table 2); (ii) unsuppressed Λ hyperonic Durca processes operate in the central region of an NS with the radius $R_{\text{D}} = 0.1R$ (Table 3); (iii) the same as (ii) but for $R_{\text{D}} = 0.3R$ (Table 4). For more details on the Durca processes with Λ hyperons see Appendix A.

Other parameters adopted in our calculations are presented in Table 1. These are the spin frequency of an NS (see the first column and Gusakov et al. 2014a for details), accretion rate, averaged over quiescent and active states, \dot{M}_{-10} , in units of $10^{-10} \text{ M}_{\odot}/\text{yr}$ (see the second column and the corresponding references), and the distance to the source, d , in kpc (the third column followed by the references). We also show the resonance temperature ($T_{\text{S res}}$, in units of 10^8 K) of the peak to which a given NS is assumed to be attached and the coupling parameter s corresponding to a given peak (the last two columns).

In Tables 2–4 ⁴ the first column presents α_0 multiplied by 10^7 , the second column shows how long an NS spends near the maximum value of α during each oscillation period [this is the parameter τ in days, calculated with the formula (52)], the third column contains periods of α -oscillations \hat{P} in years, given by Equation (61). The next four columns describe NS timing behavior and are discussed in Section 5.1. The last column in Tables 2–4 characterizes the efficiency of gravitational wave emission, which is discussed in Section 5.2.

One can see that, as was stated in the previous section, τ is indeed of the order of hours-months and is larger for low-temperature sources. This is so because of two reasons. First, τ roughly scales as \sqrt{s} , being thus higher by a factor of three for two low-temperature peaks which have $s = 0.01$. ⁵ Another factor further increasing this difference is the fact that at higher temperatures the function $F_2(T) = (L_{\text{cool}} - K_n \dot{M} c^2) / C_{\text{tot}}$ is generally larger at comparable accretion rates, while $\tau \propto 1/F_2(T_0)^{1/2}$. The period $\hat{P} \propto \tau$ and hence behaves similarly.

5.1 Timing

Typical timing behaviour of an NS climbing a peak is the following. Most of the time the stellar spin frequency and its derivative are not affected by the r modes and are determined by the external torque (accretion and spin-down torques due to, e.g., magneto-dipole losses). Spin frequency derivatives at this stage, averaged over quiescent and active phases, $\langle \dot{\nu}_{\text{acc}} \rangle$, are presented in the fourth column of Tables 2–4. To evaluate $\langle \dot{\nu}_{\text{acc}} \rangle$ we (for definiteness) neglected magneto-dipole losses and

⁴ Tables 2–4 correspond to fiducial value $\alpha_{\text{th}} = \alpha_{\text{th}}^{\text{fid}} = 10^{-12}$. Equations (47), (52), and (61) allow one to rescale them to an arbitrary α_{th} according to the formulas $\tau \approx \tau^{\text{fid}} k^{\text{fid}}/k$, $\hat{P} \approx \hat{P}^{\text{fid}} k/k^{\text{fid}}$, $|\Delta\nu| \approx |\Delta\nu^{\text{fid}}| k/k^{\text{fid}}$, $\sqrt{\hat{P}}(h_0) \approx \sqrt{\hat{P}^{\text{fid}}(h_0)} \sqrt{k/k^{\text{fid}}}$, and $\dot{\nu}_{\text{max}} = \langle \dot{\nu}_{\text{acc}} \rangle + k^2 (\langle \dot{\nu} \rangle - \langle \dot{\nu}_{\text{acc}} \rangle)$. Here τ^{fid} , \hat{P}^{fid} , $|\Delta\nu^{\text{fid}}|$, and $\sqrt{\hat{P}^{\text{fid}}(h_0)}$ are the values from Tables 2–4, $k \approx \sqrt{2[\log(5\alpha_0) - \log \alpha_{\text{th}}]}$ and $k^{\text{fid}} \approx \sqrt{2[\log(5\alpha_0) - \log \alpha_{\text{th}}^{\text{fid}}]}$. This scaling is applicable if $\alpha_{\text{max}} \approx k\alpha_0 \leq \alpha_{\text{sat}}$. The amplitude α_0 and spin frequency derivatives $\langle \dot{\nu}_{\text{acc}} \rangle$ and $\langle \dot{\nu} \rangle$ do not depend on α_{th} .

⁵ To show it we present $\partial H(T, \Omega)/\partial T|_{T_0, \Omega_0}$ entering the expression for τ (52) as $\partial H(T, \Omega)/\partial T|_{T_0, \Omega_0} \approx 8(sT_{\text{res}})^{-1} |\tau_{\text{GR}}|^{-1} (\tau_{\text{MF}}/|\tau_{\text{GR}}|)^{1/2} \propto s^{-1}$, where τ_{MF} is the mutual friction damping time of the superfluid mode. To derive this expression we used the formulas of Section IVB of Gusakov et al. 2014a and considered a limiting case $x \rightarrow -\infty$.

Table 2. Parameters of NS oscillations near the peak. No direct Urca.

Source	α_0 $\times 10^7$	τ [days]	\hat{P} [yrs]	$\langle \dot{\nu}_{\text{acc}} \rangle$ $\times 10^{14}$ [Hz sec $^{-1}$]	$\dot{\nu}_{\text{max}}$ $\times 10^{14}$ [Hz sec $^{-1}$]	$\langle \dot{\nu} \rangle$ $\times 10^{14}$ [Hz sec $^{-1}$]	$ \Delta\nu $ $\times 10^6$ [Hz]	$\sqrt{\hat{P}} \langle h_0 \rangle$ $\times 10^{24}$ [Hz $^{-1/2}$]
4U 1608-522	1.6	5.8	0.57	6.8	-3.0	6.4	0.049	2.1
SAX J1750.8-2900	2.3	5.1	0.52	3.8	-13	3.2	0.074	1.6
EXO 0748-676	2.8	8.2	0.85	3.8	-11	3.3	0.10	1.8
Aql X-1	2.2	11	1.1	7.5	-0.66	7.2	0.078	2.5
SWIFT J1749.4-2807	3.6	11	1.1	3.8	-11.3	3.2	0.14	2.4
SAX J1748.9-2021	2.7	36	3.7	3.4	0.55	3.3	0.088	1.7
IGR J17498-2921	3.0	72	7.5	3.8	2.0	3.7	0.11	2.1
KS 1731-260 ^a	—	—	—	—	—	—	—	—
IGR J00291-5934	0.12	103	8.1	0.094	0.058	0.092	0.0032	0.45
MXB 1659-298 ^a	—	—	—	—	—	—	—	—
XTE J1751-305 ^b	—	—	—	—	—	—	—	—

^a The equilibrium temperature is higher than the observed one. Direct Urca process is required.

^b Equilibrium temperature is “inside” the low-temperature peak, thus this NS spins up in the stability region.

Table 3. Parameters of NS oscillations near the peak. Direct Urca in 0.1*R*.

Source	α_0 $\times 10^7$	τ [days]	\hat{P} [yrs]	$\langle \dot{\nu}_{\text{acc}} \rangle$ $\times 10^{14}$ [Hz sec $^{-1}$]	$\dot{\nu}_{\text{max}}$ $\times 10^{14}$ [Hz sec $^{-1}$]	$\langle \dot{\nu} \rangle$ $\times 10^{14}$ [Hz sec $^{-1}$]	$ \Delta\nu $ $\times 10^6$ [Hz]	$\sqrt{\hat{P}} \langle h_0 \rangle$ $\times 10^{24}$ [Hz $^{-1/2}$]
4U 1608-522	25	0.33	0.040	6.8	-3.0×10^3	-83	0.85	8.8
SAX J1750.8-2900	28	0.37	0.046	3.8	-3.1×10^3	-89	1.0	5.8
EXO 0748-676	40	0.53	0.066	3.8	-3.4×10^3	-96	1.6	7.0
Aql X-1	40	0.54	0.067	7.5	-3.4×10^3	-92	1.6	11
SWIFT J1749.4-2807	51	0.70	0.088	3.8	-3.6×10^3	-102	2.2	9.4
SAX J1748.9-2021	28	3.2	0.39	3.4	-3.5×10^2	-7.2	0.98	5.6
IGR J17498-2921	41	4.9	0.61	3.8	-3.8×10^2	-7.7	1.7	8.2
KS 1731-260	3.6	14	1.5	2.8	-14	2.6	0.20	2.6
IGR J00291-5934	0.67	17	1.6	0.094	-1.2	0.043	0.019	1.1
MXB 1659-298 ^a	—	—	—	—	—	—	—	—
XTE J1751-305	1.8	99	9.9	0.11	-0.91	0.076	0.087	1.5

^a The equilibrium temperature is higher than the observed one. Thus Durca in 0.1*R* is not sufficient for this NS.

used the following simplified relation between $\langle \dot{\nu}_{\text{acc}} \rangle$ and \dot{M} , valid for non-magnetized NSs,

$$\langle \dot{\nu}_{\text{acc}} \rangle = \dot{M} \frac{\sqrt{GMR}}{2\pi I}. \quad (62)$$

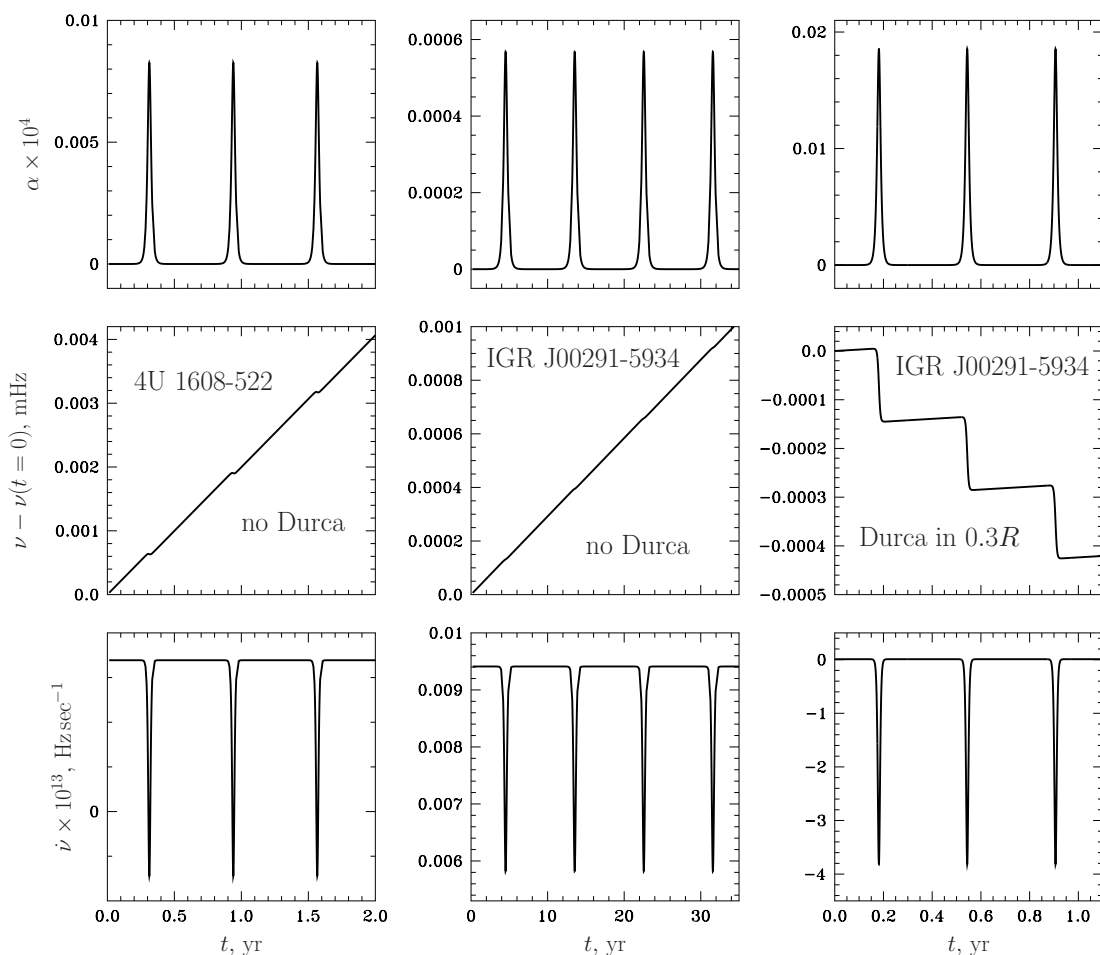
When an NS gets into the instability region the r-mode amplitude starts to grow and soon approaches its maximum value. NS affected by r-mode torque spins down rapidly at this stage. The fifth column in the Tables presents the value of the spin frequency derivative when r-mode amplitude is in its maximum, $\dot{\nu}_{\text{max}}$. This rapid spin down lasts until α is high, that is during the period of time τ . Finally, the sixth column contains the spin frequency derivative $\langle \dot{\nu} \rangle$, averaged over the large number of α -oscillation periods.

In observations a sudden spin down due to the action of the r-mode torque, lasting the time τ , can be interpreted as an anti-glitch. The sizes of the “anti-glitches” can be estimated as $|\Delta\nu| \approx (\langle \dot{\nu}_{\text{acc}} \rangle - \dot{\nu}_{\text{max}})\tau$; they are presented in the seventh column of the Tables. Using Equations (2), (3), (20), and (53) it is easy to show that $|\Delta\nu|$ can be expressed as $|\Delta\nu| \approx 3(L_{\text{cool}} - K_n \dot{M} c^2) \hat{P} / (2\pi I \Omega)$. This formula implies that the rotation energy losses during an “anti-glitch” are three times larger than the energy emitted by an NS during the whole α -oscillation period, \hat{P} . As far as r-modes do not affect the spin frequency evolution in the remaining time, the average spin down rate is the same as in the absence of α -oscillations [see Equations (16), (17) and, e.g., equation (2) of Chugunov et al. 2014]; thus the main effect of α -oscillations on the timing is concentration of all r-mode spin down in narrow time intervals $\sim \tau$. Typically, these “anti-glitches” are rather small (the values from the Tables lie in the interval $5.3 \times 10^{-12} < |\Delta\nu/\nu| < 2.3 \times 10^{-8}$) and can contribute to the timing noise.

In Fig. 4 we show examples of time dependencies of the r-mode amplitude α (top panels), spin frequency ν (middle panels) and its derivative $\dot{\nu}$ (bottom panels). Three left panels show these functions for the pulsar 4U 1608-522, assuming no Durca processes operating in the star; middle panels — for the pulsar IGR J00291-5934 again without Durcas; right panels — for the same pulsar IGR J00291-5934, but with Λ -hyperonic Durca allowed in the central region of a star with the radius

Table 4. Parameters of NS oscillations near the peak. Direct Urca in $0.3R$.

Source	α_0 $\times 10^7$	τ [days]	\hat{P} [yrs]	$\langle \dot{\nu}_{\text{acc}} \rangle$ $\times 10^{14}$ [Hz sec $^{-1}$]	$\dot{\nu}_{\text{max}}$ $\times 10^{14}$ [Hz sec $^{-1}$]	$\langle \dot{\nu} \rangle$ $\times 10^{14}$ [Hz sec $^{-1}$]	$ \Delta\nu $ $\times 10^6$ [Hz]	$\sqrt{\hat{P}}(h_0)$ $\times 10^{24}$ [Hz $^{-1/2}$]
4U 1608-522	131	0.061	8.1×10^{-3}	6.8	-8.8×10^4	-2.4×10^3	4.6	20
SAX J1750.8-2900	148	0.069	9.3×10^{-3}	3.8	-9.2×10^4	-2.5×10^3	5.4	14
EXO 0748-676	206	0.098	0.013	3.8	-1.0×10^5	-2.7×10^3	8.5	16
Aql X-1	209	0.10	0.014	7.5	-1.0×10^5	-2.7×10^3	8.7	27
SWIFT J1749.4-2807	265	0.13	0.018	3.8	-1.1×10^5	-2.8×10^3	12	22
SAX J1748.9-2021	146	0.59	0.079	3.4	-1.0×10^4	-2.8×10^2	5.3	13
IGR J17498-2921	213	0.91	0.12	3.8	-1.1×10^4	-3.0×10^2	9.0	19
KS 1731-260	20	2.3	0.28	2.8	-6.0×10^2	-15	1.2	6.5
IGR J00291-5934	3.4	3.1	0.33	0.094	-38	-1.2	0.10	2.6
MXB 1659-298	3.9	4.4	0.46	3.2	-30	2.0	0.13	1.2
XTE J1751-305	9.3	18	2.0	0.11	-32	-0.92	0.49	3.6


Figure 4. R-mode amplitude (top panels), spin frequency (middle panels), and spin-down rate (bottom panels) as functions of time for (from left to right): (a) 4U 1608-522 without Durca, (b) IGR J00291-5934 without Durca, (c) IGR J00291-5934 with Λ -hyperonic Durca allowed for $r \leq 0.3R$.

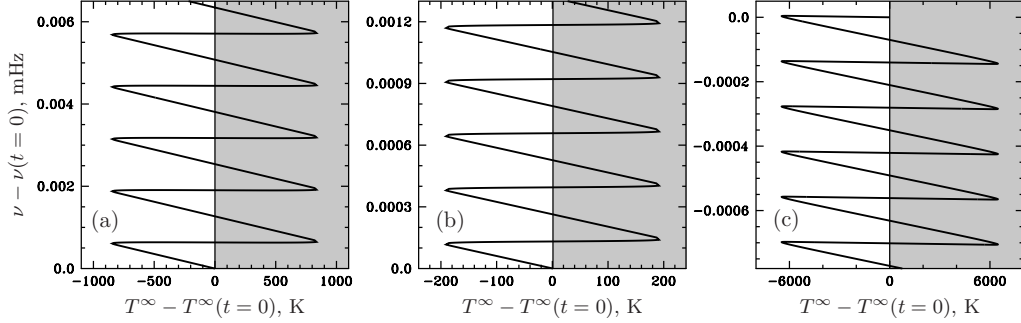


Figure 5. Oscillations of the evolutionary track near the instability curve. Shown are variations of the rotation frequency (in millihertz) and internal temperature (in Kelvins) starting from some initial moment of time $t = 0$, for the following sources: (a) 4U 1608-522, the time interval is ~ 3 years, without Durca; (b) IGR J00291-5934, the time interval is ~ 45 years, without Durca; (c) again IGR J00291-5934, the time interval is ~ 2 years, now with Λ -hyperonic Durca allowed for $r \leq 0.3R$, see the text for details.

$R_D = 0.3R$. One can see that the pulsar 4U 1608-522 exhibits short periods (several days) of rapid spin down due to the action of the r -mode torque, which are repeated every $\hat{P} = 0.63$ yr.⁶ When Durca processes are forbidden, every $\hat{P} = 9.0$ yr pulsar IGR J00291-5934 exhibits periods (lasting several dozens of days) of enhanced r -mode torque, which results in some decrease of NS spin up rate (the torque is too weak to spin down the star). Enhanced cooling makes the “anti-glitches” more pronounced and shortens the time τ of violent spin down as well as α -oscillation period, because $\hat{P} \approx (33 \div 48)\tau \propto 1/F_2(T_0)^{1/2}$ [see Equations (61) and (52)]. Thus, when Λ -hyperonic Durca processes are open in the central region of a star, the pulsar IGR J00291-5934 exhibits several days spin-down episodes with well pronounced “anti-glitch”. α -oscillation period in this case equals $\hat{P} = 0.35$ yr. One can see that α -oscillation periods obtained in numerical calculations (and given above) are slightly lower than those presented in the Tables and calculated with the approximate formula (61). The corresponding evolutionary tracks of the three particular NS models described here are presented in three panels of Fig. 5.

One more thing should be mentioned in relation with the Tables described above. From Table 4 it follows that the high-temperature sources, which are assumed to climb one of the two high-temperature peaks (centered at 10^8 K and 1.5×10^8 K) require a really high r -mode amplitude to maintain their temperature *if* Durca processes are allowed in the substantial part of their cores. However, high values of r -mode amplitude result in the strong NS deceleration (see the sixth column in Table 4) that could be ruled out by timing analysis (see Mahmoodifar & Strohmayer 2013). Moreover, such a strong neutrino cooling (and hence NS deceleration) rises a question: How did an NS get to the observed frequency? In our scenario a star typically gets there by climbing up a stability peak⁷. Assuming that an NS has climbed the peak up to the observed value of Ω we automatically imply that the r mode braking torque was not too strong, so that a sufficiently high accretion rate (e.g., $\dot{M}_{\text{acc high}} \sim 10^{-8} M_\odot/\text{yr}$ with corresponding $\dot{\Omega}_{\text{acc high}}$), that probably took place in the past, could spin the star up. This assumption imposes the following “spin up” upper limit on α_0 at the stage of strong accretion, when NS was spinning up,

$$\alpha_{\text{su}} = \sqrt{\frac{\dot{\Omega}_{\text{acc high}}}{G(T_0, \Omega_0)\Omega_0}}, \quad (63)$$

where we used Equation (17). The value of α_{su} is about 4×10^{-6} for $\nu = 600$ Hz and scales with rotation frequency as $\propto \nu^{-3.5}$ [this scaling follows from the Equations (5), (11), (62) and the fact that $\tau_{\text{Diss}} = |\tau_{\text{GR}}|$ at the edge of the peak, see Gusakov et al. 2014a)⁸. At the same time the thermal balance condition (20) dictates the value of α_0 . For example, if 4U 1608-522 was accreting at $\dot{M}_{\text{acc high}} \sim 10^{-8} M_\odot/\text{yr}$ in the past, α_0 for this source was $\alpha_0 = 1.30 \times 10^{-5}$ if $R_D = 0.3R$.⁹ Thus α_0 was higher than α_{su} , which means that 4U 1608-522 could not climb up the peak at the current cooling rate. There is, however, a possibility that Durca processes were closed in the past for the pulsar 4U 1608-522 and had opened (due to

⁶ The accurate treatment of the accretion episodes can violate the strict periodicity, but will not affect other results. The same is true for other numerical examples considered here.

⁷ This condition is not necessary if we could allow for a possibility that an NS has never climbed up a peak but only descended it. This could be a reasonable assumption for not too rapidly rotating NSs ($\nu \lesssim 400$ Hz).

⁸ Here, for definiteness, we employed the simplest expression for the accretion torque (62) that can be strongly modified by accounting for the magnetic field.

⁹ One can see that at the stage of strong accretion α_0 was slightly lower than that calculated in Table 4 for the current accretion rate, the same is predicted by Equations (10) and (20). However, the difference is very small, because neutrino cooling with $R_D = 0.3R$ is much stronger than the deep crustal heating rate even for $\dot{M}_{\text{acc high}} \sim 10^{-8} M_\odot/\text{yr}$ (the function $F_2(T_0)$ defined by (10) and entering the thermal balance condition (20), is practically independent of the accretion rate).

the mass accretion) only after this source has climbed up the peak to a rather high frequency. Only in the case of such a fine tuning one can allow the Durca processes to operate in a substantial part of 4U 1608-522 currently. It is clear from the consideration above that detailed analysis of the hottest NSs in LMXBs could put tight constraints on the neutrino emission due to Durca processes in the cores of these stars.

5.2 Gravitational radiation

First, let us discuss whether gravitational waves can, in principle, be detected on long time scales (involving large number of α -oscillation periods, $t \gg \hat{P}$). Detection statistics respond to integrated signal power (Owen 2010), thus to rms (root-mean-square) value of α , i.e. to the quantity α_0 (see Section 3). Since α_0 is defined by approximate thermal balance of a star, Equation (20), the analysis in this case should be essentially the same as that of Mahmoodifar & Strohmayer (2013), where it was assumed that an NS undergoes r-mode oscillations at some (small) saturation amplitude and is in thermal equilibrium during these oscillations.

Assume that we know the frequency of gravitational waves ω , which equals to the r-mode frequency in the inertial frame, and is given, in the Newtonian limit, by the formula, $\omega = 4/3 \Omega$ (for $l = m = 2$ r mode)¹⁰. In this case gravitational waves can be detected if (see, e.g., equation (6) of Watts, Krishnan, Bildsten, & Schutz 2008 and Jaranowski, Królak, & Schutz 1998)

$$\left(\frac{1}{t} \int_0^t h_0(t')^2 dt' \right)^{1/2} \sqrt{t} = \left(\int_0^t h_0(t')^2 dt' \right)^{1/2} > 11.4 \sqrt{S_n(\omega)}, \quad (64)$$

where $S_n(\omega)$ is the power spectral density of the detector noise; t is the duration of signal collection; $h_0(t')$ is the time-dependent intrinsic strain amplitude, which equals (see, e.g., Owen 2010)

$$h_0(t') = \sqrt{\frac{8\pi}{5}} \frac{1}{d} \omega^3 \alpha(t' - \Delta t) M R^3 \tilde{J}, \quad (65)$$

where d is the distance to the source, and Δt is the duration of gravitational signal propagation from the source to the detector; $c = G = 1$ in this formula (G is the gravitational constant). For long-term observations (involving large number of oscillation periods of α , $t \gg \hat{P}$) the rms value of α equals α_0 , and $h_0(t')$ in formula (64) can be replaced with its rms value $\langle h_0 \rangle$, given by equation (65) with $\alpha(t' - \Delta t) = \alpha_0$. Obviously, the higher α_0 is the more favorable is detection. α_0 can be rather high (and detectable by, e.g., Advanced LIGO) for most of the sources, especially if Durca processes are operating in their cores, see Tables 2–4. However, too high values of α_0 would result in a very rapid spin-down of an NS, and may contradict the timing measurements (future or existing) of NSs in LMXBs. See detailed analysis of this issue in Mahmoodifar & Strohmayer (2013).

The registration of gravitational waves during a shorter period of time, particularly when $\alpha(t' - \Delta t)$, and hence $h_0(t')$ stays near its maximum in the course of oscillations, cannot improve statistics, since any collection of even weak signal contributes to the statistics [see Equation (64)]. However, registration of the signal near the maximums of α could substantially decrease the time cost (or computational cost) of the observation with the minimal losses in sensitivity. Moreover, under certain conditions, the period of α -oscillations, \hat{P} , can be pretty large, up to 10 years (see the third columns in Tables 2–4). In this case the duration of observations will be inevitably shorter than \hat{P} . Then, if the period of observations is chosen properly (its duration is of the order of τ and α reaches its maximum during the period of observation), the gravitational wave can be detected if [see Equation (64)]

$$\left(\int_0^t h_0(t')^2 dt' \right)^{1/2} \sim h_{0 \max} \sqrt{\tau} \sim \langle h_0 \rangle \sqrt{\hat{P}} > 11.4 \sqrt{S_n(\omega)}, \quad (66)$$

where $h_{0 \max}$ is given by (65) with $\alpha(t' - \Delta t) = \alpha_{\max}$. To derive (66) we used the fact that most of the α -oscillation period α is negligibly small and r mode excites for a time of the order of τ , and adopted an approximate equality (53). Notice that \hat{P} in Equation (66) can be as large as several years, but one does not need to process the signal collected during the whole period \hat{P} , it is only necessary to process the signal collected during the time interval τ , which is $\sqrt{2(k^2 - \log k^2)} k \approx (33 \div 48)$ times shorter than \hat{P} . The values of $\langle h_0 \rangle \sqrt{\hat{P}}$ are presented in the last column of Tables 2–4.

To choose the correct time for the detection of gravitational signal we either should be sufficiently lucky or need to know α -oscillation parameters (when exactly r-mode amplitude reaches the maximum). These parameters can, in principle, be found from the peculiarities in timing behavior of a given source, see Section 5.1.

¹⁰ General relativistic corrections modify this relation and introduce substantial uncertainties in ω (see, e.g., Andersson et al. 2014; Idrisy et al. 2015 and references therein). However, direct measurements of NS spin frequency Ω and frequency ω_X of X-ray emission modulation from the NS surface due to perturbations of the surface by r mode would allow to determine ω as $\omega = \omega_X - 2\Omega$. We probably already have one such candidate with both frequencies measured, this is the pulsar XTE J1751-305, see Strohmayer & Mahmoodifar (2014a) (see also Strohmayer & Mahmoodifar 2014b).

6 α -OSCILLATIONS VS EXISTING OBSERVATIONS

Since gravitational waves have not yet been detected, the only observational manifestation of α -oscillations in existing observations can be found in timing of NSs.

Some of the NSs in LMXBs are X-ray pulsars showing pulsations from time to time (during outbursts). For this reason their timing parameters are poorly constrained. The best measurements of timing parameters were done for the source HETE J1900.12455 (see Patruno 2012). This source showed a strong decrease in the rotation frequency time derivative, $\dot{\nu}$, on a short timescale of the order of 26 ± 4 days. Patruno (2012) fitted this change of $\dot{\nu}$ as an exponential decay and interpreted it as a manifestation of the magnetic field burial. However, the same observational data can also be interpreted (and fitted) as α -oscillations discussed in this paper. Unfortunately, the quality of the observational data does not allow one to distinguish which model is correct and which is not (private communication with A. Patruno). Additional X-ray observation of this source with high temporal resolution would be highly desirable.

On the other hand, the timing behavior of millisecond radio pulsars is often measured very precisely and an upcoming projects like SKA (Kramer & Stappers 2015; Tauris et al. 2015) will increase the number of such pulsars. The scenario proposed by Gusakov et al. (2014b,a) admits that after accretion stage finishes and an NS becomes a millisecond radio pulsar it may still stay attached to one of the stability peaks (there are, however, other possibilities, see Gusakov et al. 2014b,a). This peak should be a low-temperature one, because observations indicate that non-accreting millisecond pulsars are relatively cool.¹¹ NS, attached to the peak, may experience α -oscillations. However, to our best knowledge, there are no known peculiarities in timing behavior of millisecond pulsars, which can be attributed to the timing features discussed here. We can not exclude that these peculiarities are masqueraded by the pulsar timing noise. The large periods of α -oscillations and small amplitudes of the accompanying “anti-glitches” in cold NSs with low L_{cool} argue in favour of this assumption¹². However, if timing of all millisecond pulsars is indeed unaffected by α -oscillations, this can indicate that either (i) all millisecond pulsars are stable with respect to r-modes (for example, due to evolution in a nontrivial r-mode instability window, see, e.g., appendix D in Gusakov et al. 2014a or due to some unknown dissipation mechanism, which makes the r-mode instability irrelevant for the physics of NSs) or (ii) all unstable millisecond pulsars are pinned to the stability peaks, which are sufficiently wide, so that α -oscillations do not excite for them (see a corresponding discussion after the expression 41 in Section 3)¹³. The latter assumption looks very natural, because the low-temperature peaks should be wider than the high-temperature ones, as is confirmed by calculations of the spectra of non-rotating superfluid NSs (Gusakov et al. 2013; Gualtieri et al. 2014). It is interesting to ask how wide should be a peak to allow an NS to climb it up/down without oscillations? For example, to make the motion of IGR J00291-5934 along the left edge of the stability peak stable (i.e., to make $\gamma(A_0) < 0$) it is enough to increase the coupling parameter s to the value $s = 0.04$ (by a factor of 4), which looks to be realistic (this estimate is made for the case when Durca is open in the region $r \leq R_D = 0.1R$).

Even if non-accreting millisecond pulsars are unaffected by α -oscillations, some NSs in LMXBs (accreting millisecond pulsars), which are attached to sharper peaks centered at higher temperatures, still can be unstable with respect to α -oscillations and thus should exhibit them. To check this possibility we need more X-ray observations with high temporal resolution that can be achieved by future missions such as LOFT (Feroci et al. 2012), NICER (Gendreau et al. 2012), and SRG (Merloni et al. 2012). Another opportunity to detect α -oscillations can be associated with the recently discovered transitional millisecond pulsars, which are switching between rotation- and accretion-powered states [currently, three of such objects are known: PSR J1023+0038 ($\nu \approx 592.4$ Hz, Archibald et al. 2009; Stappers et al. 2014), IGR J18245–2452 ($\nu \approx 254.3$ Hz, Papitto et al. 2013), and XSS J12270–4859 ($\nu \approx 593.0$ Hz, Roy et al. 2015)]. In a rotation-powered state these NSs are observed as radio pulsars, giving a chance to study their timing properties precisely. The accretion-powered state guarantees that these pulsars can not be too cold, and thus likely to be affected by r-mode instability and α -oscillations. For example, the red-shifted surface temperature of PSR J1023+0038 can be as large as 5×10^5 K (Homer et al. 2006; Bogdanov et al. 2011). It corresponds to the internal temperature $T^\infty = (1.5 \div 3) \times 10^7$ K, implying that PSR J1023+0038 can be on the stability peak. Its timing behavior was reported as ‘complex’ by Archibald et al. (2013) and can be influenced by α -oscillations. The reliable registration of α -oscillations would confirm the crucial role of the resonance interaction of oscillation modes in the

¹¹ Due to this reason their surface temperatures are still not measured (only X-ray emission from polar caps is registered for some of them). The only exception is the pulsar PSR J0437–4715 (spin frequency $\nu \approx 173.7$ Hz) with the redshifted surface temperature $(1.25 \div 3.5) \times 10^5$ K, corresponding to the emitting radius $15 \div 7.8$ km (Durant et al. 2012); even the largest estimate of the surface temperature for this pulsar corresponds to $T^\infty < 2 \times 10^7$ K, which is too low to make PSR J0437–4715 r-mode unstable.

¹² Note that the most stable millisecond pulsars (whose timing noise is extensively studied in relation to the problem of gravitational wave detection) are not very rapid rotators and can be stable with respect to r-mode excitation (for example, the fastest pulsar in NANOGrav project, PSR J1909–3744, has $\nu \approx 339$ Hz, see, e.g., Demorest et al. 2013).

¹³ Formally, there is an additional possibility that the unstable millisecond pulsars are not associated with the stability peaks. However, it requires extremely small r-mode saturation amplitudes (see, e.g., Alford & Schwenzer 2015), which seems to be very unlikely, see a footnote 9 in Gusakov et al. (2014a).

evolution of NSs in LMXBs (Gusakov et al. 2014b,a). The measurements of α -oscillation parameters (such as the period of oscillations, \hat{P}) would provide us with a new powerful tool to constrain the properties of superdense matter.

7 CONCLUSIONS

We showed that when an NS climbs the stability peak according to the scenario proposed by Gusakov et al. (2014b,a), its parameters can undergo *nonlinear* oscillations near their equilibrium values (α -oscillations). We studied these oscillations analytically and determined their key parameters such as the oscillation period and amplitude. We also found a rigorous criterion showing when α -oscillations become unstable. For fully developed unstable α -oscillations we demonstrated that, most of the α -oscillation period, the amplitude of r-mode α stays negligibly small and increases only for a short time of the order of hours-months (depending on parameters) by a factor of about $5 \div 6$ in comparison to its root mean square value. Thus, the spin frequency derivative, which is not affected by r modes most of the time, dramatically decreases, generally approaching large negative values, when α becomes large. This results in small “anti-glitches” (for NSs in LMXBs considered here their sizes lie within the range $5.3 \times 10^{-12} < |\Delta\nu/\nu| < 2.3 \times 10^{-8}$ for the adopted parameters), which typically last hours-months depending on the model. This fact can substantially affect timing analysis of rapidly rotating NSs (radio-, X-ray and transitional millisecond pulsars), in particular it potentially can be useful for interpretation of timing behavior of NSs in LMXBs, such as HETE J1900.12455 (Patruno 2012) and IGR J00291-5934 (Patruno 2010). Moreover, the very existence of oscillations of the r-mode amplitude α could substantially decrease the time cost of gravitational signal detection from LMXBs, because collection of the signal during the time period τ when α is close to its maximum (typically, hours-months) results in almost the same sensitivity as collection of the signal during the whole α -oscillation period ($\sim 40\tau$). The identification of α -oscillations in observations would confirm the scenario of NS evolution in LMXB proposed in Gusakov et al. (2014a,b) and would show that r modes are crucially important for understanding of rapidly rotating NSs. It would also open a new independent way to constrain the properties of superdense matter of NS cores by measuring α -oscillation parameters.

APPENDIX A: COOLING RATE OF AN NS

To calculate the luminosity in the absence of Durca processes (let us denote it L_{noDurca}) we use an approximate formula, which expresses L_{noDurca} as a function of the internal (redshifted) stellar temperature T^∞ , see formula (A1) in appendix A of Gusakov et al. (2014a). This formula fits numerical results for the luminosity obtained with the relativistic cooling code, described in detail by Gusakov et al. (2004, 2005) and Yakovlev & Pethick (2004). To calculate L_{noDurca} , essentially the same microphysics input was used as in Gusakov et al. (2004), namely, the parameterization by Heiselberg & Hjorth-Jensen (1999) of APR EOS (Akmal et al. 1998) was employed, and an NS with the mass $M = 1.4M_\odot$ was considered.

It is generally believed that hyperons appear in the NS matter at densities $\sim (2 - 3)\rho_0$, where $\rho_0 = 2.8 \times 10^{14}$ g cm $^{-3}$ is the nuclear density (see, e.g., Weissenborn et al. 2012; Bednarek et al. 2012; Gusakov et al. 2014c and references therein). This threshold for hyperon appearance is rather low which means that substantial fraction of NSs (probably) host hyperons in their cores. Most of the modern models predict that the first hyperons to appear with increasing density is Λ hyperons (see, e.g., Weissenborn et al. 2012; Bednarek et al. 2012; Gusakov et al. 2014c). It is quite likely that the superfluid gap for them is very low (Tanigawa et al. 2003; Takatsuka et al. 2006; Wang & Shen 2010) so that Λ hyperons are normal at temperatures relevant to NSs in LMXBs. According to many microscopic models, protons are also non-superconducting at sufficiently high densities (e.g., Page et al. 2009). As soon as Λ hyperons appear, the very powerful direct Urca process, $\Lambda \rightarrow p + l + \bar{\nu}_l$, and the inverse one, $p + l \rightarrow \Lambda + \nu_l$, start to operate in the NS interiors (here l stands for a lepton, electron or muon). The corresponding neutrino emissivity was calculated by Prakash et al. (1992); Yakovlev et al. (2001). Here we present the total emissivity due to the reactions with electrons and muons and assume that it is not suppressed by the proton and/or Λ hyperon superfluidity.

$$Q \approx 8 \times 10^{27} \left(\frac{n_e}{n_0} \right)^{1/3} \frac{m_\Lambda^* m_p^*}{m_n^2} T_9^6 r_{\Lambda p} \text{ erg cm}^{-3} \text{ sec}^{-1}, \quad (\text{A1})$$

where $n_0 = 0.16 \text{ fm}^{-3}$ is the nuclear number density, n_e is the electron number density, $T_9 \equiv T/10^9 \text{ K}$, $r_{\Lambda p} = 0.039$, m_Λ^* , and m_p^* are the effective masses for Λ hyperons and protons, respectively, m_n is the mass of a free neutron. In all numerical calculations we adopt $m_\Lambda^* = 0.7m_\Lambda$ ($m_\Lambda = 1115.63 \text{ MeV}$) and $m_p^* = 0.7m_n$. As long as the emissivity is not too sensitive to the actual value of the electron number density n_e , we assume $n_e = 0.25n_0$ throughout the whole region where the Durca processes are open (it is a good approximation for the central part of a star). This is a typical value of n_e near the threshold density of Λ hyperon appearance (Gusakov et al. 2014c).

Using Q from the equation (A1) we calculate (or better to say, estimate) the neutrino luminosity due to the Λ hyperon

Durca processes as

$$L_{\text{Durca}} = Q \frac{4}{3} \pi R_{\text{D}}^3, \quad (\text{A2})$$

where R_{D} is the radius of the inner part of the stellar core where Λ hyperons are present; we treat R_{D} as a free parameter and consider three cases: $R_{\text{D}} = 0$ (no Λ hyperons), $R_{\text{D}} = 0.1R$, and $R_{\text{D}} = 0.3R$. The resulting luminosity (cooling rate) L_{cool} is calculated as a sum of L_{noDurca} and L_{Durca} , $L_{\text{cool}} = L_{\text{noDurca}} + L_{\text{Durca}}$.

ACKNOWLEDGMENTS

We are grateful to Alessandro Patruno for correspondence and some clarifying comments on the timing behavior of HETE J1900.12455 and to Cristóbal Espinoza and Y.A. Shibano for discussions. This study was partially supported by RFBR (grants 14-02-00868-a and 14-02-31616-mol-a), and by RF president programme (grants MK-506.2014.2 and NSh-294.2014.2).

REFERENCES

- Akmal A., Pandharipande V. R., Ravenhall D. G., 1998, *Phys. Rev. C*, 58, 1804
 Alford M. G., Han S., Schwenzer K., 2015, *Phys. Rev. C*, 91, 055804
 Alford M. G., Schwenzer K., 2015, *Mon. Not. R. Astron. Soc.*, 446, 3631
 Andersson N., 1998, *Astrophys. J.*, 502, 708
 Andersson N., Jones D. I., Ho W. C. G., 2014, *Mon. Not. R. Astron. Soc.*, 442, 1786
 Andersson N., Kokkotas K. D., 2001, *International Journal of Modern Physics D*, 10, 381
 Archibald A. M., Kaspi V. M., Hessels J. W. T., Stappers B., Janssen G., Lyne A., 2013, *ArXiv e-prints* 1311.5161
 Archibald A. M. et al., 2009, *Science*, 324, 1411
 Bednarek I., Haensel P., Zdunik J. L., Bejger M., Mařka R., 2012, *Astron. Astrophys.*, 543, A157
 Bogdanov S., Archibald A. M., Hessels J. W. T., Kaspi V. M., Lorimer D., McLaughlin M. A., Ransom S. M., Stairs I. H., 2011, *Astrophys. J.*, 742, 97
 Bondarescu R., Teukolsky S. A., Wasserman I., 2007, *Phys. Rev. D*, 76, 064019
 Bondarescu R., Teukolsky S. A., Wasserman I., 2009, *Phys. Rev. D*, 79, 104003
 Brink J., Teukolsky S. A., Wasserman I., 2004, *Phys. Rev. D*, 70, 121501
 Brown E. F., 2000, *Astrophys. J.*, 531, 988
 Brown E. F., Bildsten L., Rutledge R. E., 1998, *Astrophys. J. Lett.*, 504, L95
 Chugunov A. I., Gusakov M. E., 2011, *Mon. Not. R. Astron. Soc.*, 418, L54
 Chugunov A. I., Gusakov M. E., Kantor E. M., 2014, *Mon. Not. R. Astron. Soc.*, 445, 385
 Degenaar N. et al., 2014, *Astrophys. J.*, 791, 47
 Demorest P. B. et al., 2013, *Astrophys. J.*, 762, 94
 Durant M., Kargaltsev O., Pavlov G. G., Kowalski P. M., Posselt B., van Kerkwijk M. H., Kaplan D. L., 2012, *Astrophys. J.*, 746, 6
 Feroci M. et al., 2012, *Experimental Astronomy*, 34, 415
 Friedman J. L., Morsink S. M., 1998, *Astrophys. J.*, 502, 714
 Gendreau K. C., Arzoumanian Z., Okajima T., 2012, in *Society of Photo-Optical Instrumentation Engineers (SPIE) Conference Series*, Vol. 8443, *Society of Photo-Optical Instrumentation Engineers (SPIE) Conference Series*
 Glampedakis K., Andersson N., 2006, *Phys. Rev. D*, 74, 044040
 Gualtieri L., Kantor E. M., Gusakov M. E., Chugunov A. I., 2014, *Phys. Rev. D*, 90, 024010
 Gusakov M. E., Chugunov A. I., Kantor E. M., 2014a, *Phys. Rev. D*, 90, 063001
 Gusakov M. E., Chugunov A. I., Kantor E. M., 2014b, *Physical Review Letters*, 112, 151101
 Gusakov M. E., Haensel P., Kantor E. M., 2014c, *Mon. Not. R. Astron. Soc.*, 439, 318
 Gusakov M. E., Kaminker A. D., Yakovlev D. G., Gnedin O. Y., 2004, *Astron. Astrophys.*, 423, 1063
 Gusakov M. E., Kaminker A. D., Yakovlev D. G., Gnedin O. Y., 2005, *Mon. Not. R. Astron. Soc.*, 363, 555
 Gusakov M. E., Kantor E. M., Chugunov A. I., Gualtieri L., 2013, *Mon. Not. R. Astron. Soc.*, 428, 1518
 Haskell B., 2015, *International Journal of Modern Physics E*, 24, 1541007
 Haskell B., Degenaar N., Ho W. C. G., 2012, *Mon. Not. R. Astron. Soc.*, 424, 93
 Haskell B., Glampedakis K., Andersson N., 2014, *Mon. Not. R. Astron. Soc.*, 441, 1662
 Heinke C. O., Jonker P. G., Wijnands R., Deloye C. J., Taam R. E., 2009, *Astrophys. J.*, 691, 1035
 Heinke C. O., Jonker P. G., Wijnands R., Taam R. E., 2007, *Astrophys. J.*, 660, 1424
 Heiselberg H., Hjorth-Jensen M., 1999, *Astrophys. J. Lett.*, 525, L45
 Heyl J. S., 2002, *Astrophys. J. Lett.*, 574, L57

- Ho W. C. G., Andersson N., Haskell B., 2011, *Physical Review Letters*, 107, 101101
- Ho W. C. G., Lai D., 2000, *Astrophys. J.*, 543, 386
- Homer L., Szkody P., Chen B., Henden A., Schmidt G., Anderson S. F., Silvestri N. M., Brinkmann J., 2006, *AJ*, 131, 562
- Idrisy A., Owen B. J., Jones D. I., 2015, *Phys. Rev. D*, 91, 024001
- Jaranowski P., Królak A., Schutz B. F., 1998, *Phys. Rev. D*, 58, 063001
- Kantor E. M., Gusakov M. E., 2011, *Phys. Rev. D*, 83, 103008
- Kinney J. B., Mendell G., 2003, *Phys. Rev. D*, 67, 024032
- Kramer M., Stappers B., 2015, *Advancing Astrophysics with the Square Kilometre Array (AASKA14)*, 36, arxiv 1507.04423
- Levin Y., 1999, *Astrophys. J.*, 517, 328
- Levin Y., Ushomirsky G., 2001, *Mon. Not. R. Astron. Soc.*, 324, 917
- Linares M. et al., 2011, *The Astronomer's Telegram*, 3568, 1
- Lindblom L., Mendell G., 2000, *Phys. Rev. D*, 61, 104003
- Lowell A. W. et al., 2012, *Astrophys. J.*, 749, 111
- Mahmoodifar S., Strohmayer T., 2013, *ApJ*, 773, 140
- Mendell G., 2001, *Phys. Rev. D*, 64, 044009
- Merloni A. et al., 2012, *ArXiv 1209.3114*
- Owen B. J., 2010, *Phys. Rev. D*, 82, 104002
- Owen B. J., Lindblom L., Cutler C., Schutz B. F., Vecchio A., Andersson N., 1998, *Phys. Rev. D*, 58, 084020
- Page D., Lattimer J. M., Prakash M., Steiner A. W., 2009, *Astrophys. J.*, 707, 1131
- Papitto A. et al., 2013, *Nature*, 501, 517
- Patruno A., 2010, *Astrophys. J.*, 722, 909
- Patruno A., 2012, *Astrophys. J. Lett.*, 753, L12
- Potekhin A. Y., Fantina A. F., Chamel N., Pearson J. M., Goriely S., 2013, *Astron. Astrophys.*, 560, A48
- Prakash M., Prakash M., Lattimer J. M., Pethick C. J., 1992, *Astrophys. J. Lett.*, 390, L77
- Rieutord M., 2001a, *Astrophys. J.*, 550, 443
- Rieutord M., 2001b, *Astrophys. J.*, 557, 493
- Roy J. et al., 2015, *Astrophys. J. Lett.*, 800, L12
- Stappers B. W. et al., 2014, *Astrophys. J.*, 790, 39
- Strohmayer T., Mahmoodifar S., 2014a, *Astrophys. J.*, 784, 72
- Strohmayer T., Mahmoodifar S., 2014b, *Astrophys. J. Lett.*, 793, L38
- Takatsuka T., Nishizaki S., Yamamoto Y., Tamagaki R., 2006, *Progress of Theoretical Physics*, 115, 355
- Tanigawa T., Matsuzaki M., Chiba S., 2003, *Phys. Rev. C*, 68, 015801
- Tauris T. M. et al., 2015, *Advancing Astrophysics with the Square Kilometre Array (AASKA14)*, 39, arxiv 1501.00005
- Wagoner R. V., Hennawi J. F., Liu J., 2001, in *American Institute of Physics Conference Series*, Vol. 586, 20th Texas Symposium on relativistic astrophysics, Wheeler J. C., Martel H., eds., pp. 781–786
- Wang Y. N., Shen H., 2010, *Phys. Rev. C*, 81, 025801
- Watts A. L., Krishnan B., Bildsten L., Schutz B. F., 2008, *Mon. Not. R. Astron. Soc.*, 389, 839
- Weissenborn S., Chatterjee D., Schaffner-Bielich J., 2012, *Nuclear Physics A*, 881, 62
- Wijnands R., Rol E., Cackett E., Starling R. L. C., Remillard R. A., 2009, *Mon. Not. R. Astron. Soc.*, 393, 126
- Yakovlev D. G., Kaminker A. D., Gnedin O. Y., Haensel P., 2001, *Phys. Rep.*, 354, 1
- Yakovlev D. G., Pethick C. J., 2004, *Ann. Rev. Astron. Astrophys.*, 42, 169
- Yoshida S., Lee U., 2001, *Astrophys. J.*, 546, 1121